Geochemistry Geophysics Geosystems G3
AN ELECTRONIC JOURNAL OF THE EARTH SCIENCES
Published by AGU and the Geochemical Society

Article
Volume 3, Number 6
20 June 2002
10.1029/2001GC000251
ISSN: 1525-2027

Trace of the Kerguelen mantle plume: Evidence from seamounts between the Kerguelen Archipelago and Heard Island, Indian Ocean

Dominique Weis
Département des Sciences de la Terre et de l'Environnement, Université Libre de Bruxelles CP160/02, Avenue F.D. Roosevelt, 50, B-1050 Brussels, Belgium (dweis@ulb.ac.be)

Currently at Earth and Ocean Sciences, University of British Columbia, Vancouver, V6T-1Z4, Canada (dweis@eos.ubc.ca)

Frederick A. Frey
Department of Earth, Atmospheric and Planetary Sciences, Massachusetts Institute of Technology, Cambridge, Massachusetts 02139, USA (fafrey@mit.edu)

Roland Schlich, Marc Schaming, and Raymond Montigny
Ecole et Observatoire des Sciences de la Terre (ULP), Institut de Physique du Globe de Strasbourg (UMR CNRS 7516), 67084 Strasbourg, France (mschaming@eost.u-strasbg.fr; Raymond.montigny@eost.u-strasbg.fr)

Dimitri Damasceno and Nadine Mattielli
Département des Sciences de la Terre et de l'Environnement, Université Libre de Bruxelles CP160/02, Avenue F.D. Roosevelt, 50, B-1050 Brussels, Belgium (ddamasce@mac.com; nmattiel@ub.ac.be)

Kirsten E. Nicolaysen
Department of Earth, Atmospheric and Planetary Sciences, Massachusetts Institute of Technology, Cambridge, Massachusetts 02139, USA

Currently at Département des Sciences de la Terre et de l'Environnement, Université Libre de Bruxelles CP160/02, Avenue F.D. Roosevelt, 50, B-1050 Brussels, Belgium (knicol@ksu.edu)

James S. Scoates
Département des Sciences de la Terre et de l'Environnement, Université Libre de Bruxelles CP160/02, Avenue F.D. Roosevelt, 50, B-1050 Brussels, Belgium (jscoates@ulb.ac.be)

Currently at Earth and Ocean Sciences, University of British Columbia, Vancouver, V6T-1Z4, Canada (jscoates@eos.ubc.ca)

[1] The gravity and bathymetric highs on the Kerguelen Plateau in the southern Indian Ocean between the Kerguelen Archipelago and Heard Island are seamounts formed of Miocene alkalic basalts similar to those found on the islands. Dredging during the Kerimis survey cruise recovered >1 ton of mostly basaltic rocks. One of the dredges (D6) yielded a large volume of in situ alkalic picritic pillow basalts, the first picritic lavas recovered that are related to the Kerguelen plume. K-Ar and ^{40}Ar-^{39}Ar ages are between 18 and 21 Ma for all but one sample, and these ages are only slightly younger than the main phase of volcanism on the archipelago. The dredged lavas form three distinct groups based on chemical and isotopic compositions. Incompatible element abundance ratios overlap with compositional groups defined by lavas from both the Kerguelen Archipelago and Heard Island indicating that alkalic volcanism in this region of the Kerguelen

Plateau has been spatially diverse. Olivine and picritic basalts have Sr and Nd isotopic characteristics similar to most of the lavas exposed on the archipelago and those proposed for the Kerguelen plume. However, compared to Kerguelen Archipelago lavas, the picritic basalts have relatively low $^{206}Pb/^{204}Pb$ which is a characteristic of Cretaceous basalt forming some parts of the Kerguelen Plateau. We propose that the apparent age trend of the lavas from 34 Ma in the Northern Kerguelen Plateau (ODP Leg 183, Site 1140) to 24–30 Ma on the Kerguelen Archipelago to 18–21 Ma on the dredged submarine volcanoes, and even possibly to recent volcanism on Heard and McDonald Islands, may correspond to the Tertiary hot spot track of the Kerguelen plume.

Components: 12,583 words, 11 figures, 7 tables.

Keywords: Kerguelen; trace elements; isotopes; mantle plume; hot spot track; picrites; geochemistry.

Index Terms: 1025 Geochemistry: Composition of the mantle; 1040 Geochemistry: Isotopic composition/chemistry; 1065 Geochemistry: Trace elements (3670).

Received 11 October 2001; **Revised** 19 February 2002; **Accepted** 19 February 2002; **Published** 20 June 2002.

Weis, D., F. A. Frey, R. Schlich, M. Schaming, R. Montigny, D. Damasceno, N. Mattielli, K. E. Nicolaysen, and J. S. Scoates, Trace of the Kerguelen mantle plume: Evidence from seamounts between Kerguelen Archipelago and Heard Island, Indian Ocean, *Geochem. Geophys. Geosyst.*, *3*(6), 10.1029/2001GC000251, 2002.

1. Introduction

[2] The Kerguelen mantle plume has produced 15.2 to 24.1 × 10^6 km^3 of basaltic magmas (minimum and maximum volumes assuming off- and on-ridge emplacement, respectively [*Coffin and Eldhom*, 1994]) for at least 120 million years [*Weis et al.*, 1989a; *Barron et al.*, 1989; *Schlich et al.*, 1989]. The Kerguelen plume played an important role in generating major tectonic features in the Indian Ocean [e.g., *Weis et al.*, 1991; *Frey et al.*, 2000a] and subsequently in the genesis of geochemical anomalies in Indian Ocean floor basalts [*Dosso et al.*, 1988; *Mahoney et al.*, 1992; *Weis and Frey*, 1996; *Graham et al.*, 1999]. The long volcanic record of the Kerguelen plume includes a large igneous province (the giant oceanic plateau Kerguelen Plateau-Broken Ridge), which may be associated with plume initiation, the >5000 km long 82–38 Ma Ninetyeast Ridge hot spot track, which is the longest linear feature on Earth that formed as the Indian Plate migrated rapidly northwards over the plume, and recently active oceanic islands (Kerguelen Archipelago, McDonald and Heard Islands) on the Antarctic Plate (Figure 1).

[3] The surface expression of the Kerguelen plume during the late Cretaceous and early Tertiary resulted in the formation of the Southern and Central Kerguelen Plateau, Broken Ridge, and Ninetyeast Ridge. In particular, Ninetyeast Ridge provides compelling evidence for the trace of the Kerguelen hot spot as the Indian plate moved northwards over the plume [*Duncan and Richards*, 1991]. The current location of the hot spot is uncertain; Eocene and younger lavas occur on both the Kerguelen Archipelago and Heard Island, which are separated by ~440 km, and there is current volcanism at McDonald Island (Figure 1). At ~34 Ma, tholeiitic basalts erupted in the location of ODP Site 1140 of Leg 183 in the northern part of the Northern Kerguelen Plateau [*Frey et al.*, 2000a; *Duncan and Pringle*, 2000; *Weis and Frey*, 2000] (Figure 2). Over 250 km to the south (Figure 1), the transitional to alkalic flood basalts that cover >85% of the Kerguelen Archipelago formed between 30 and 24 Ma [*Nicolaysen et al.*, 2000]. The younger, volumetrically minor basanites and differentiated lavas in the southeast and southern part of the Kerguelen Archipelago occur principally as dikes or plugs in the flood basalts and have ages between 10 and 6 Ma for the Upper Miocene series of the southeast Province [*Weis et al.*, 1993] and between 2 Ma and 0.1 Ma at Mount Ross [*Weis et al.*, 1998b]. The most recent volcanic activity on the Kerguelen Archipelago has been alkalic with abun-

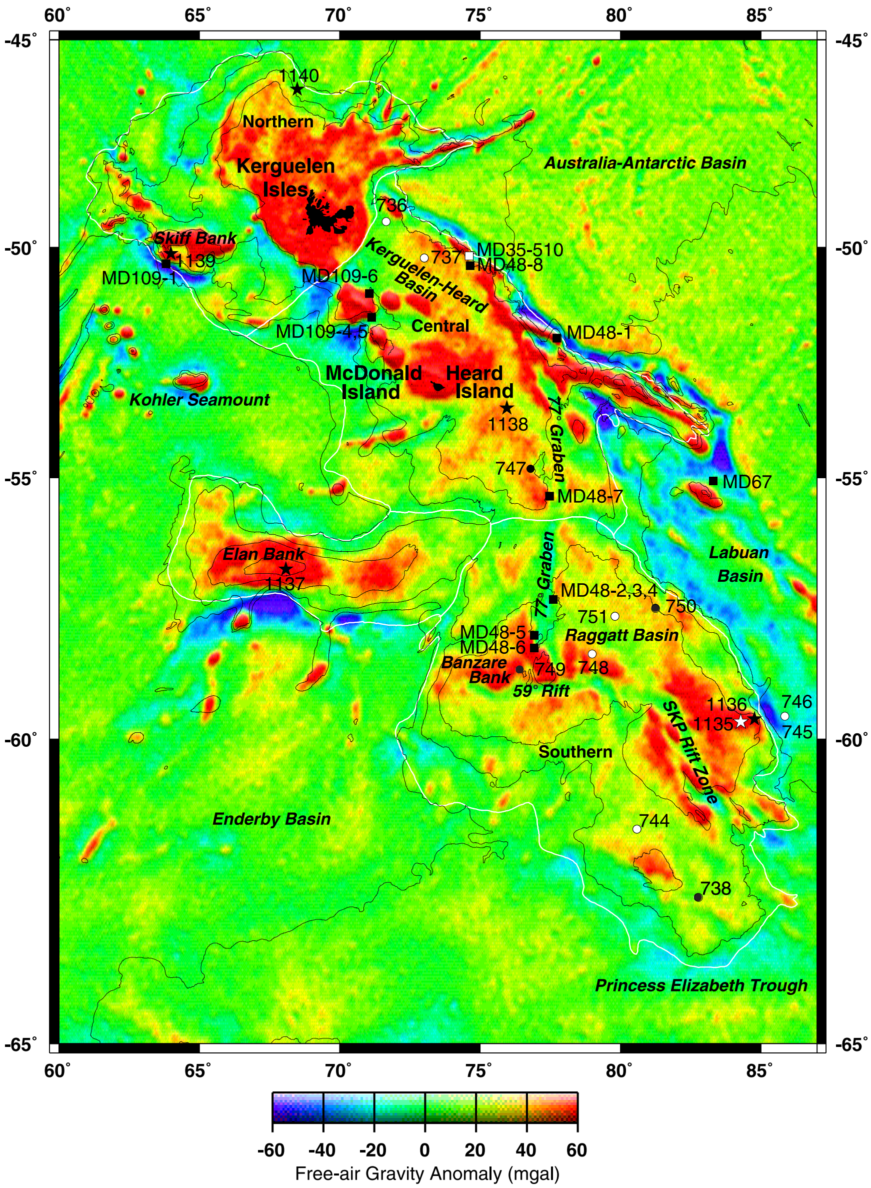

Figure 1. Map of the southeastern Indian Ocean showing major physiographic features related to the activity of the Kerguelen plume [*Coffin et al.*, 2000], as well as the drill sites of ODP Legs 119, 120 (circles) and 183 (stars) and dredge sites on the Kerguelen Plateau (squares). Black symbols indicate that basement was reached.

dant evolved lavas (trachytes and phonolites). To the south, Heard Island (Figure 2) also has a record of volcanism from middle Eocene to Recent; however, Pleistocene-Holocene lavas are volumetrically dominant [*Barling et al.*, 1994]. Both Heard Island and the nearby McDonald Island have had historic eruptions (1998). This brief geochronologic summary illustrates why there is significant uncertainty in the location of the Kerguelen hot spot and therefore in plate tectonic reconstructions of the Indian Ocean. Most plate reconstruction models locate the hot spot on the west of the Kerguelen Archipelago in order to fit Ninetyeast Ridge [*Duncan and Storey*, 1992; *Steinberger*, 2000], whereas the record of recent volcanic activity would put the hot spot beneath Heard Island.

[4] Constraining the current location of the Kerguelen hot spot is of fundamental importance, not only for understanding the history of the Kerguelen

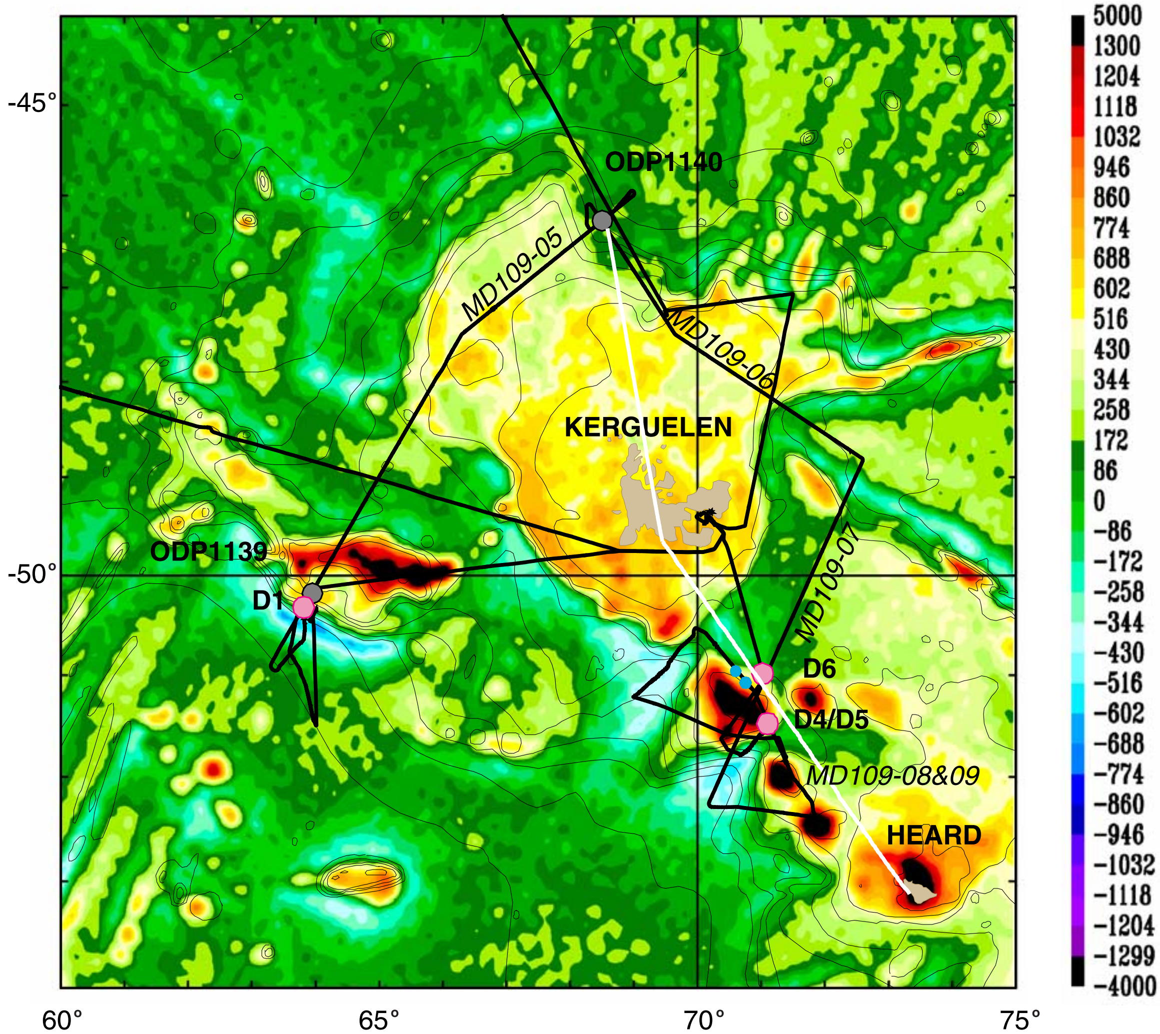

Figure 2. Satellite-derived gravity field for the Northern Kerguelen Plateau (scale in 1/10 mgals) showing the MD109-Kerimis track chart, dredge sites (pink), proposed drilling sites (cyan) and ODP Leg 183 site locations (grey). The two white lines represents the transect shown on Figure 11.

plume, but also for reconciling plate tectonic reconstructions of the Indian Ocean basin. Understanding the tectonic history of the Indian Ocean will also potentially shed light on the breakup of eastern Gondwana [*Nicolaysen et al.*, 2001] and the subsequent complex mid-ocean ridge reorganizations, which may have included one or more ridge jumps. Importantly, the Kerguelen plume is characterized by distinctive geochemical signatures, very different from those of Iceland or Hawaii [*Zindler and Hart*, 1986; *Weis et al.*, 1989b], and as such can yield unique information about the origin of mantle heterogeneities. This paper presents the first geochronologic and geochemical study of seamounts between Kerguelen Archipelago and Heard Islands. Notably the first picritic basalts related to the Kerguelen plume were recovered from one of these seamounts. The ages of dredged seamount lavas and their geochemical affinity with other Kerguelen lavas provide compelling evidence for an Oligocene-to-Recent hot spot track of the Kerguelen plume.

1.1. Kerguelen Plume and Kerguelen Plateau

[5] The 2×10^6 km^2 Kerguelen Plateau (Figure 1) has been divided into several distinct domains [*Houtz et al.*, 1977; *Schlich*, 1982; *Coffin et al.*,

1986; *Munschy et al.*, 1994]: (1) northern Kerguelen Plateau (NKP) which has shallow water depths (<1000 m) and includes the Kerguelen Archipelago, (2) central Kerguelen Plateau (CKP) which is also relatively shallow, contains a large sedimentary basin (Kerguelen-Heard Basin), and includes the volcanically active Heard and McDonald islands, (3) southern Kerguelen Plateau (SKP) which is characterized by deeper water depths (1500–2500 m), contains a major sedimentary basin (Raggatt Basin), and is tectonically more complex than the NKP and CKP, (4) Elan Bank, which extends westward from near the boundary between the CKP and the SKP and has water depths less than 2000 m, and (5) Labuan Basin, which adjoins the CKP and SKP to the east, and is a deep (>3500 m), extensively faulted, thickly sedimented (>2000 m) basin whose structure is similar to that of the main Kerguelen Plateau. The dredged seamounts are located on the NKP and northern CKP (Figure 1).

[6] Dredging and drilling of basement has yielded tholeiitic basalts with ages of 110–119 Ma for the Southern Kerguelen Plateau, 108–110 for Elan Bank, and 94–102 Ma for the central Kerguelen Plateau and Broken Ridge [*Leclaire et al.*, 1987; *Pringle and Duncan*, 2000]. The geochemical characteristics of these basalts are consistent with derivation from the Kerguelen plume [*Davies et al.*, 1989; *Weis et al.*, 1989a; *Salters et al.*, 1992; *Storey et al.*, 1992; *Coffin et al.*, 2000], but basalts from the southern tip of the plateau (Site 738) and Elan Bank (Figure 1) have geochemical signatures reflecting the presence of a continental lithospheric component [*Mahoney et al.*, 1995; *Weis et al.*, 2001]. Although the Kerguelen Archipelago, which is constructed on the northern Kerguelen Plateau, has been studied in detail [*Gautier et al.*, 1990; *Weis et al.*, 1993, 1998b; *Yang et al.*, 1998; *Frey et al.*, 2000b; *Nicolaysen et al.*, 2000], the submarine basement of the northern Kerguelen Plateau had not been sampled prior to this study and the subsequent ODP drilling Leg 183 [*Frey et al.*, 2000a].

1.2. Kerimis Survey Cruise: Dredge Locations and Descriptions

[7] New multichannel seismic reflection data were collected in March 1998 during the Kerimis (Kerguelen, Imagerie Multifaisceau et Imagerie Sismique) survey cruise of the French research vessel Marion Dufresne 2 [*Schlich et al.*, 1998]. Five transects, ∼2000 km in total, were shot over the northern Kerguelen Plateau and over several large seamounts located to the south and to the west of the Kerguelen Archipelago (Figure 2). The first southwest-northeast transect (MD109-05) was located to the northwest of the archipelago between ODP sites 1139 and 1140. It extends southward from the northern boundary of the NKP across the submarine platform of the archipelago and crosses Leclaire Rise (or Skiff Bank) at almost a right angle. This transect and a northwest-southeast transect (MD109-06) identify a prominent basement surface, which may indicate that throughout the NKP subaerial erosion occurred before subsequent subsidence and sedimentation. A north-south transect east of the archipelago (MD109-07) crosses the deep Cretaceous Kerguelen-Heard sedimentary basin [*Schlich et al.*, 1971; *Munschy and Schlich*, 1987]. This transect and two additional transects (MD109-08 and MD109-09) cross several large seamounts with clearly defined dipping basement reflector wedges. These data coupled with results of the previous surveys (1970, 1972, and 1981) were used to identify locations for dredging during the Kerimis cruise and to survey the basement for drilling sites 1139 and 1140 of ODP Leg 183 [*Coffin et al.*, 2000].

[8] More than 1 ton of basalt was recovered from four dredge sites (Figures 1 and 2). Dredge 1 (D1: 50°21′S-63°48′E) on the Northern Kerguelen Plateau, west of the Kerguelen Archipelago, was located on the flank of Skiff Bank and collected 200 kg of samples of diverse rock types including aphyric basaltic to trachybasaltic lavas, microgabbroic to alkali granitic intrusive rocks, and sedimentary rocks. With the exception of the rare fresh basalts (<5%), all the samples are small (10–20 cm), rounded and coated by Fe-Mn. These rocks will be discussed elsewhere in conjunction with studies of lavas recently recovered from Skiff Bank at ODP Leg 183 Hole 1139 [*Frey et al.*, 2000a; *Kieffer et al.*, 2000].

[9] Dredges 4 (D4: 51°31′S-71°09′E) and 5 (D5: 51°31′S-71°08′E) were on the northern part of the

central Kerguelen Plateau on the most northerly of the seamounts that are distributed linearly between the Kerguelen Archipelago and Heard Island (Figure 2). D4 and D5 traversed the lower and upper southeast flank of this structure. These dredges recovered ~700 kg of basalt, with features reflecting an in situ origin (fresh broken surfaces, columnar shapes, minimal Mn crusts). These basalts have abundant centimeter-size olivine/clinopyroxene phenocrysts that distinguish them from the basalts of the Kerguelen Archipelago where plagioclase phenocrysts are relatively common [*Gautier et al.*, 1990].

[10] Dredge 6 (D6: 51°01′S-071°04′E) was on the northeast flank of the same structure and collected >1 ton of very fresh samples, mainly picritic pillow basalts with abundant olivine phenocrysts. The fresh broken surfaces of the pillows indicate that these are in situ samples. The convex surfaces of the pillows are Fe-Mn-coated glass. Vesicles are not abundant, but pipe vesicles 5–15 cm in length radiate from the pillow cores.

2. Analytical Techniques

2.1. Mineral Chemistry

[11] Olivine and clinopyroxene mineral compositions (Tables A1 and A2) were determined using a CAMECA SX100 electronprobe (CNRS – Blaise Pascal University, Clermont-Ferrad, France) with the following settings: accelerating voltage, 15 kV; beam current, 15 nA; beam size, 3 μm; counting time, 15 s; and a ZAF correction factor. Calibration was made with natural and synthetic standards.

2.2. K-Ar and ^{40}Ar-^{39}Ar Dating

[12] Details on analytical techniques for the K-Ar and ^{40}Ar-^{39}Ar dating is given by *Montigny et al.* [1988] and *Henry et al.* [1998] The set of constants recommended by *Steiger and Jäger* [1977] was used for age calculation. The 120–150 mg aliquots of standard biotite LP6 (129 Ma) were utilized as flux monitors. Uncertainties representing estimates of analytical precision are quoted as 2σ and were calculated using the procedure of *Cox and Dalrymple* [1967] for K-Ar conventional dates and using that of *Albarède* [1976] for ^{40}Ar-^{39}Ar dates.

2.3. Major and Trace Element Concentrations

[13] Abundances of the major elements and the trace elements Rb, Sr, Ba, V, Ni, Zn, Ga, Y, Zr, Nb, La, and Ce were determined by X-ray fluorescence (XRF) at the University of Massachusetts, Amherst [*Rhodes*, 1996]. All reported XRF data are the mean values of duplicate analyses. Abundances of the trace elements Sc, Cr, Co, Hf, Ta, Th, and several rare earth elements were determined by instrumental neutron activation at MIT [*Ila and Frey*, 2000]. The accuracy and precision of these techniques were discussed by *Rhodes* [1996] and *Ila and Frey* [2000].

2.4. Sr, Nd, and Pb Isotopic Compositions

[14] Samples for Sr, Nd, and Pb isotope analyses were selected to encompass the entire range of chemical compositions. The chemical procedure used was similar to that described by *Weis et al.* [1987] with improvements as discussed by *Weis and Frey* [1991]. All of the samples were acid-leached to remove secondary or alteration phases. Total blank values were <1 ng for all three isotopic systems considered. Such values are negligible in view of the elemental concentrations in the samples. Sr and Nd isotopic compositions were measured on single Ta filaments and triple Re-Ta filaments, respectively, in the dynamic mode on a VG Sector 54 multicollector mass spectrometer with an internal precision better than 1×10^{-5} unless specified in Table 4. Sr isotopic ratios were normalized to $^{86}Sr/^{88}Sr = 0.1194$ and Nd isotopic ratios (for isotopes 147, 146, 145, 144, 143, and 142, measured as metal), to $^{146}Nd/^{144}Nd = 0.7219$. The average $^{87}Sr/^{86}Sr$ value of the NBS 987 Sr standard was 0.71027 ± 2 ($2\sigma_m$ on 48 samples) and analyses of the Rennes Nd standard yielded $^{143}Nd/^{144}Nd = 0.51196 \pm 1$ ($2\sigma_m$ on 39 samples). Pb isotopic compositions were measured on single Re filaments using the H_3PO_4-silica gel technique. All Pb isotopic ratios were corrected for mass fractionation (0.12 ± 0.04% per amu) on the basis of 72 analyses of the NBS 981 Pb standard for a

temperature range between 1090°C and 1150°C. Between-run precisions were better than ~0.1% for $^{206}Pb/^{204}Pb$ and $^{207}Pb/^{204}Pb$ and better than ~0.15% for $^{208}Pb/^{204}Pb$. The quality of a complete replicate analysis can be evaluated by sample D4-33, which was analyzed twice because of its unusual composition.

2.5. Hf Isotopic Compositions

[15] Extraction of Hf was performed at the Université Libre de Bruxelles. Hf isotope analyses were carried out on the multicollector plasma-source mass spectrometer (P54) at the Ecole Nationale Supérieure de Lyon, following the analytical procedure of *Blichert-Toft et al.* [1997]. All measured Hf isotopic ratios were corrected for W and Ta, Lu and Yb interferences at masses 180 and 176, respectively, by monitoring the isotopes ^{182}W, ^{181}Ta, ^{175}Lu, ^{173}Yb and normalized for mass fractionation to $^{179}Hf/^{177}Hf$ of 0.7325 using an exponential law. During the period of data collection, eighteen analyses of the JMC175 Hf standard gave an unweighted mean for $^{176}Hf/^{177}Hf$ of 0.28216 ± 1 (standard deviation).

2.6. He Isotopic Compositions

[16] Sample MD109-07 D6 88 was crushed to less than 2 mm diameter using a disk mill and sieved to obtain a size fraction between 0.8 and 2 mm. A Frantz magnetic separator was used to concentrate the olivine before handpicking of the most pristine phenocrysts using a binocular microscope. The olivine separate was abraded for several hours in an air-abrader to remove adhering groundmass and alteration minerals. After a final microscopic inspection, the abraded olivines were weighed and rinsed with 4N HNO_3 and water in an ultrasonic bath. The sample was dried with a final rinse with acetone and loaded into a clean crusher for in vacuo analysis by the 90° sector mass spectrometer at the Woods Hole Oceanographic Institution [e.g., *Kurz et al.*, 1996].

3. Results

3.1. Age of the Seamounts

[17] K-Ar and ^{40}Ar-^{39}Ar measurements were made on whole rock samples (Tables 1 and 2). The combined use of the two methods was essential to evaluate the loss of neutron-induced $^{39}Ar_K$ owing to recoil from fine-grained phases or glass [*Seidemann*, 1977], which results in overestimates of the ages. Evaluating the geological meaning of K-Ar and ^{40}Ar-^{39}Ar dates for submarine basalts can be difficult. We use two criteria: first the comparison between the K-Ar conventional age and the ^{40}Ar-^{39}Ar integrated age, and second the shape of the ^{40}Ar-^{39}Ar release spectrum.

[18] The ^{40}Ar-^{39}Ar release spectra are displayed in Figure 3. The salient features of the results are as follows:

1. Olivine basalts from D5, which contain a significant amount of glass in the matrix, give K-Ar ages from 16.5 to 17.7 Ma, whereas they yield Ar-Ar integrated ages of around 19.5 Ma, all within error of each other. Two of the samples (D5-44a and D5-44b) display inverse-shaped spectra (i.e., the high temperature steps correspond to the lowest ages, while the third (D5-42) reveals a hump-shaped one). Both types of release spectrum are commonly attributed to irradiation in the nuclear reactor, which causes $^{39}Ar_K$ redistribution owing to recoil in glassy or cryptocrystalline matrix [*Turner et al.*, 1997].
2. Picritic basalts (D6) with a glassy matrix yield fairly concordant K-Ar ages from 13.8 to 14.8 Ma, except one sample that indicates a somewhat older date of 19.0 Ma. They yield fairly concordant Ar-Ar integrated ages, between 18.7 and 21.4 Ma. The shapes of the release patterns are variable: flat for the most part of D6-88 and D6-89, inverse for D6-87, and hump-shaped for D6-85.
3. Basalt D4-37, which has olivine phenocrysts in a well-crystallized matrix, yields a K-Ar date of 21.0 ± 0.6 Ma. Its degassing pattern is characterized by an anomalously old age for the initial step, 220 ± 20 Ma, and a well-defined plateau with an age of 21.9 ± 0.2 Ma. It indicates an integrated age of 23.9 ± 0.4 Ma, which if calculated without the initial step, becomes 21.3 ± 0.6 Ma.
4. Basalt D4-33, which has pyroxene and olivine phenocrysts in a fresh crystalline matrix, yields a K-Ar age of 0.72 ± 0.25 Ma and an Ar-Ar integrated age of 1.6 ± 0.7 Ma. The degassing pattern is staircase-type.

[19] All ^{40}Ar-^{39}Ar ages are slightly older than the K-Ar ages for the same sample. Inspection of the

Table 1. K-Ar Ages on the Kerimis Dredged Basalts[a]

Sample	Rock Type	K_2O, weight %	$^{40}Ar^*_{\times 100}$ total ^{40}Ar	rad. ^{40}Ar, 10^{-11}mole/g	Age, Ma	±2σ, Ma
D4-33	basalt	0.823	4.7	0.0853	0.72	0.25
D4-37	basalt	2.091	40.2	6.360	21.0	0.6
D5-42	olivine basalt	2.331	48.5	5.558	16.5	0.5
D5-44a	olivine basalt	2.035	48.0	5.199	17.7	0.5
D5-44b	olivine basalt	2.141	57.1	5.232	16.9	0.5
D6-85	picritic basalt	1.077	12.2	2.173	14.0	0.8
D6-87	picritic basalt	1.363	25.0	2.925	14.8	0.6
D6-88	picritic basalt	0.904	12.7	2.492	19.0	1.0
D6-89	picritic basalt	1.282	11.1	2.557	13.8	0.9

[a] The $^{40}K/K$ total = 1.167×10^{-4} mole/mole; $\lambda\beta = 4.962 \times 10^{-10}$ a^{-1}; $\lambda\epsilon = 0.581 \times 10^{-10}$ a^{-1}.

inverse isochron diagrams reveals no significant occurrence of excess argon. The Ca/K release is normal for all types of basalt. The ratio is low in the initial step, rises more or less gradually with temperature, and rises dramatically in the final step, displaying high values.

[20] Olivine basalts (D5) display ^{40}Ar-^{39}Ar integrated ages, which are 15% higher than the conventional K-Ar ages. This difference cannot be explained either by a systematic bias in conventional K-Ar measurement of standard rocks nor by heterogeneity of the standard LP6 in ^{40}Ar-^{39}Ar dating as the samples were measured against three different aliquots of that standard. Accordingly, we consider a 15% $^{39}Ar_K$ loss during irradiation to be likely. The concordant K-Ar dates suggest that the samples are contemporaneous. Given the significant amount of glass, we view the highest value, 17.7 ± 0.5 Ma, as the minimum age for the time of emplacement of these basalts. The freshness of the samples and the moderate loss of ^{39}Ar during irradiation, however, suggests that the $^{40}Ar^*$ loss by the matrix should not have been severe. Therefore we propose an age of emplacement bracketed between 17.7 and 20–21 Ma, plateau ages yielded by D5-44a and D5-42, respectively.

[21] The difference between the conventional K-Ar ages and ^{40}Ar-^{39}Ar ages for three of the picritic basalts (D6) suggests that they underwent 30–40% ^{39}Ar loss during irradiation, while sample D6-88 did not suffer appreciably. Therefore we focus on D6-88 to appraise the geological age of the picritic basalts. The last steps of the degassing pattern with low ages are indicative of $^{39}Ar_K$ redistribution during irradiation. Nevertheless, this redistribution occurred without significant argon loss as exemplified by the concordance of the K-Ar conventional age with the ^{40}Ar-^{39}Ar age. Consequently, we propose a minimum age of 19.1 ± 1.0 Ma for the emplacement. The freshness of sample D6-88 and

Table 2. Summary of ^{40}Ar-^{39}Ar Results on the Kerimis Dredged Basalts

Sample	Integrated Date in Ma ± 2σ	Plateau Date in Ma ± 2σ	$^{36}Ar/^{40}Ar$ versus $^{39}Ar/^{40}Ar$ date in Ma ± 2σ	Initial $^{40}Ar/^{36}Ar$
D4-33	1.60 ± 0.7	1.63 ± 0.42[a]	1.56 ± 0.74[b]	297 ± 3
D4-37	23.9 ± 0.4	21.9 ± 0.40	21.9 ± 0.70	296 ± 12
D5-42	19.1 ± 0.4	20.4 ± 0.30	20.2 ± 0.50	301 ± 8.8
D5-44a	20.0 ± 0.5	21.2 ± 0.50	21.0 ± 0.60	295 ± 4
D5-44b	19.3 ± 0.5			
D6-85	18.7 ± 1.0			
D6-87	21.4 ± 2.0			
D6-88	19.2 ± 1.3	20.7 ± 1.30	20.3 ± 2.60	295 ± 3
D6-89	19.3 ± 1.6			

[a] "Plateau age" determined with two steps representing 90% of the released $^{39}Ar_K$.
[b] Isochron determined with five steps.

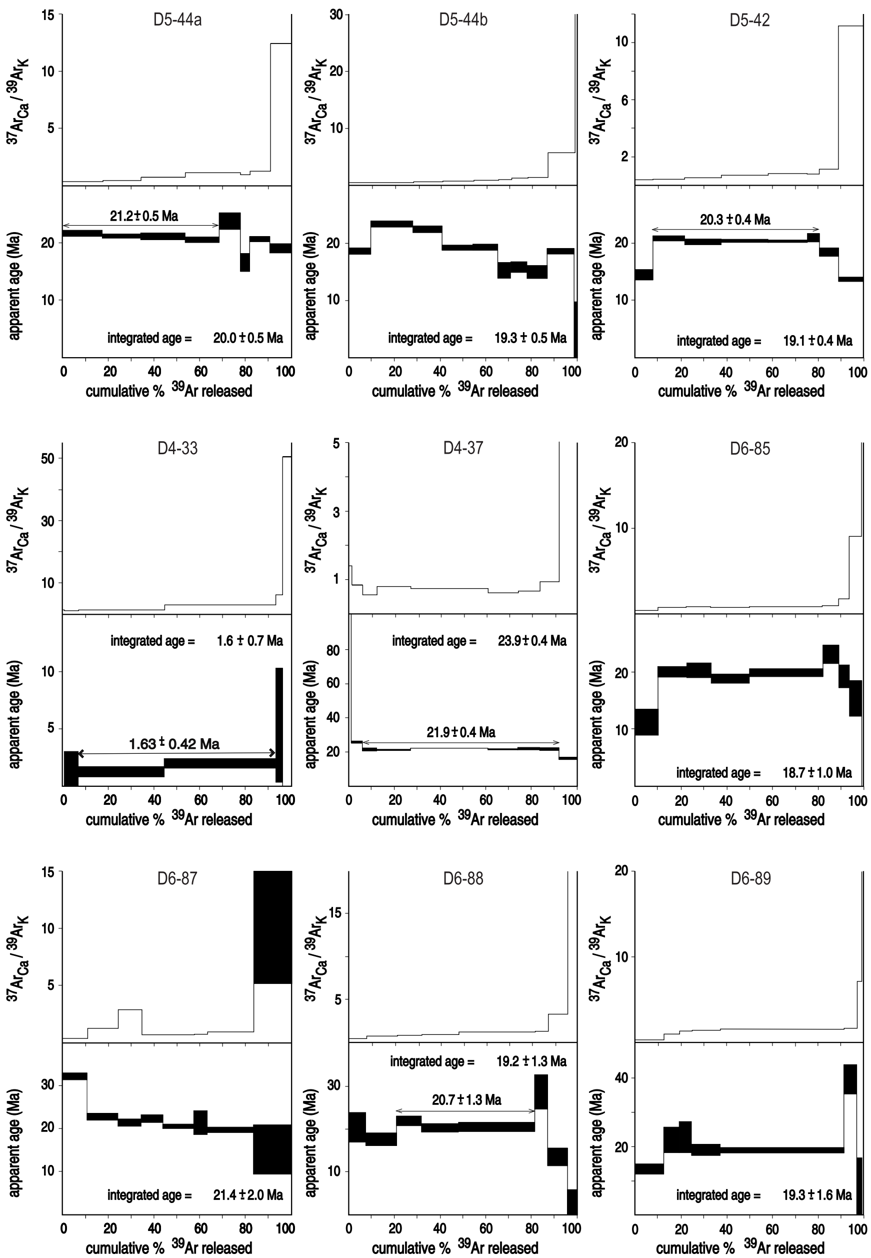

Figure 3. ^{40}Ar-^{39}Ar age spectrum plots for Kerimis dredged basalts. The uncertainties are quoted at two standard deviation.

the probable absence of $^{39}Ar_K$ loss during irradiation are reasons to assume that the glass matrix of the basalt retained $^{40}Ar^*$ completely. Hence the age of emplacement should not exceed 20 Ma.

[22] The anomalously high age of the first step of basalt sample D4-37 (220 ± 20 Ma), which amounts to 1.3% of the released $^{39}Ar_K$, is probably due to significant $^{39}Ar_K$ loss by the surface of the grains. If we discard this step the integrated Ar-Ar age becomes 21.3 ± 0.6 Ma, in good agreement with the K-Ar conventional age of 21.0 ± 0.6 Ma, which is proposed as the time of emplacement, given the freshness and the minor amount of glass of the basalt.

[23] Basalt D4-33 yields a conventional K-Ar age, 0.72 ± 0.25 Ma, somewhat different from the ^{40}Ar-^{39}Ar age, 1.6 ± 0.7 Ma. The well-crystallized nature of the matrix precludes any significant loss

of $^{39}Ar_K$ during irradiation. The isochron diagram does not reveal an initial $^{40}Ar/^{36}Ar$ ratio different from the air ratio and precludes the existence of extraneous argon. Therefore we choose as a probable age of emplacement the "plateau age" given by the two consecutive steps contributing to 90% of the released $^{39}Ar_K$ and showing the lowest errors, 1.63 ± 0.42 Ma.

[24] In summary, the seamounts dredged between the Kerguelen Archipelago and Heard Island sampled three types of basalts of comparable age, 18–21 Ma, slightly younger than the last phases of alkalic flood basalt volcanism on the archipelago [*Nicolaysen et al.*, 2000]. The abundance of glass in the matrix of the olivine basalts (D5) and picritic basalts (D6) does not allow for the establishment of a more detailed chronology. The 1.6 Ma basalt (D4-33) demonstrates the existence of recent activity previously undocumented in this area.

3.2. Petrology and Mineral Chemistry of the Picritic Basalts and Other Dredged Basalts

[25] All of the dredged basalts contain abundant phenocrysts of olivine ± clinopyroxene and those from D4 contain plagioclase phenocrysts. Representative olivine compositions are reported in Table A1 and representative clinopyroxene compositions are reported in Table A2. The general petrographic characteristics (rock type, vesicles, phenocryst morphology, and grain sizes) of the samples from the Kerimis MD109 dredges are summarized in Table A3. Modal abundances of phenocrysts and vesicles were determined by counting 1500 points per thin section.

[26] The picritic basalts (D6) contain 28–35 vol % olivine phenocrysts, including xenocrysts, with minor augite phenocrysts (0–1.3 vol %) (Table A3). The olivine phenocrysts (Fo_{83-84}) are large (up to 5 mm), euhedral and unzoned (Figures 4a and 4b). In contrast, the olivine xenocrysts are rounded or have irregular shapes indicative of resorption (Figures 4c and 4d) and have slightly higher Fo contents ($Fo_{85.5}$) than the equant olivine phenocrysts. Many of the xenocrysts display undulatory or patchy extinction (Figures 4c and 4d) suggesting that they have undergone solid-state deformation prior to being incorporated into the picritic lavas. None of the xenocrysts contain major dislocations or kink bands as have been documented for Hawaiian picritic basalts [*Garcia*, 1996] and for the Réunion picritic basalts [*Albarède et al.*, 1997]. Many of the olivine phenocrysts in the picritic basalts contain chromite inclusions (Figures 4a and 4e), and some phenocrysts contain melt inclusions that are typically altered, although local pristine patches of glass remain (Figure 4f). The chemistry of these chromite and glass inclusions is discussed in detail by *Borisova et al.* [2002]. The rare, euhedral clinopyroxene phenocrysts in the picritic basalts from D6 are Mg-rich ($En_{51}Fs_{07}Wo_{42}$) and Al-poor (1–3 wt % Al_2O_3), consistent with a low-pressure origin, and show only minor compositional zoning.

[27] The olivine basalts (D5) and basalts (D4) are much less porphyritic than the D6 picritic basalts (Table A3). The olivine basalts (D5) contain 2–4 vol % of skeletal and euhedral olivine phenocrysts (Fo_{78-83}) in a fine-grained groundmass of clinopyroxene and plagioclase microlites. The basalt (D4-33) is highly vesicular and contains 10 vol % of zoned plagioclase (An_{44-64}), 3 vol % of subhedral olivine (Fo_{59-70}), and 2 vol % of subhedral clinopyroxene ($En_{48}Fs_{16}Wo_{36}$) phenocrysts. Finally, the alkali basalt (D4-37) is different from all other dredged lavas having clinopyroxene more abundant than olivine (Table A3). This sample contains 3.5 vol % of zoned, fractured clinopyroxene ($En_{42-54}Fs_{17-07}Wo_{41-39}$), which appears to be xenocrystic in origin, 2 vol % of olivine phenocrysts, and 3 vol % of zoned plagioclase phenocrysts (An_{60-78}).

3.3. Major and Trace Element Compositions

[28] Major and trace element abundances were determined for nine whole rock samples (Table 3). On the basis of their typical OIB-like Ba/Rb abundance ratios (11.4–14.7) compared to the average oceanic basalt ratio of 11.6 [*Hofmann and White*, 1982], these samples have not experienced significant postmagmatic mobility of alkali metals. The D4 basalt and D6 picritic basalts plot near or on the

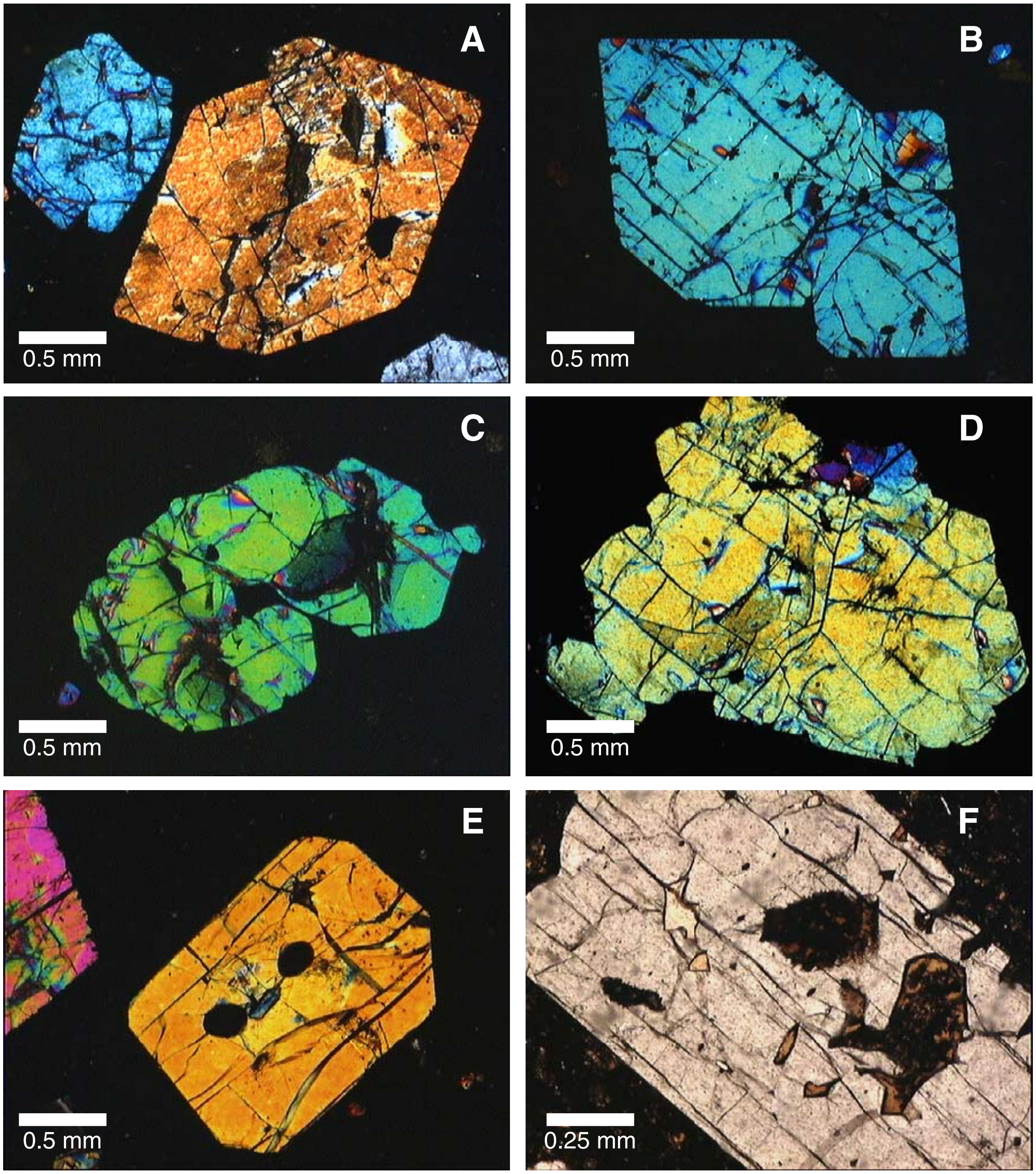

Figure 4. Photomicrographs illustrating the different types of olivine phenocrysts and xenocrysts present in the D6 picritic basalts and their inclusions. The scale is noted on each photomicrograph. Photomicrographs A–E are in crossed-polarized light and F is in plain-polarized light. A. Euhedral olivine phenocryst from sample MD109-71 showing near-perfect double terminations indicative of equilibrium crystallization. The phenocryst contains two patches of altered brown glass and a small chromite inclusion (lower right). B. Euhedral olivine phenocryst from sample MD109-89 showing excellent development of external crystal faces. C. Irregular, resorbed olivine xenocryst from the same sample (MD109-89) as the previous euhedral phenocrysts. D. Very irregular, resorbed olivine xenocryst from MD109-71. This xenocryst is also slightly deformed with the development of small subgrains along the upper margin of the main grain. E. Two rounded chromite inclusions in a single euhedral olivine phenocryst from MD109-89. F. Numerous brown glass inclusions within a single olivine phenocryst from MD109-72.

Table 3. Major and Trace Element for Kerimis Dredged Basalts[a]

Dredges	4	4	5	5	5	6	6	6	6	
Samples	33	37	42	44a	44b	85	88	87	89	BHVO-1
SiO_2	49.44	50.97	47.41	46.43	45.92	46.09	46.07	46.52	46.19	49.58
TiO_2	3.20	3.34	4.18	3.90	4.39	2.03	2.01	2.12	2.00	2.74
Al_2O_3	15.10	14.57	12.61	12.43	12.22	8.22	8.08	8.56	7.98	13.61
Fe_2O_3	12.69	10.86	13.04	12.94	13.92	13.16	13.35	13.20	13.30	12.17
MnO	0.15	0.13	0.15	0.22	0.14	0.16	0.17	0.17	0.16	0.17
MgO	5.78	5.40	7.48	7.53	7.14	19.45	20.04	18.50	20.16	7.09
CaO	8.23	8.79	9.01	10.24	9.82	7.18	6.99	7.39	6.99	11.35
Na_2O	3.71	2.74	2.68	2.80	2.84	1.45	1.50	1.49	1.43	2.40
K_2O	1.11	2.40	2.62	2.22	2.19	1.36	1.36	1.45	1.36	0.55
P_2O_5	0.62	0.57	.97	1.46	1.62	0.35	0.34	0.36	0.34	0.27
XRF										
Rb	17.8	45.7	46.2	33.8	34.6	25.3	26.7	25.4	25.6	9.2
Sr	577	660	882	842	907	422	415	409	406	388
Ba	210	468	529	498	478	321	311	310	307	139
V	183	198	209	221	213	145	152	148	144	285
Cr	108	119	281	307	321	1095	1118	1157	1155	284
Ni	87	105	177	187	163	799	754	837	847	126
Zn	140	126	167	172	229	132	137	135	132	113
Ga	27	24	23	22	22	14	14	13	13	21
Y	29.1	26.3	33.0	34.9	53.1	14.8	15.4	14.6	14.5	24.6
Zr	325	346	447	409	451	200	207	195	194	191
Nb	38.9	38.0	71.2	65.0	74.2	24.0	24.8	23.8	23.6	19.4
La	35	40	64	61	76	30	31	30	28	16
Ce	61	89	112	102	113	45	51	45	46	36
INAA										
Sc	17.5		20.5	22.8	20.7	19.2	19.3	19.1	19.0	37.2
Cr	119		272	299	285	1132	1143	1180	1130	290
Co	42.3		49.3	51.3	43.7	89.7	93.1	92.4	91.6	43.9
Hf	7.16		9.87	9.2	9.65	4.32	4.44	4.47	4.39	4.4
Ta	2.35		4.19	3.82	4.28	1.32	1.27	1.36	1.16	1.16
Th	3.17		6.76	6.0	6.7	2.40	2.28	2.41	2.36	1.07
La	29.5		59.7	57.7	71.7	25.0	24.6	24.6	23.8	15.1
Ce	69.7		129	121	131	54.7	52.2	53.4	52.0	39.7
Nd	38.3		62.0	59.6	69.4	27.0	26.2	24.9	24.8	24.4
Sm	8.88		12.4	11.6	13.4	5.25	5.20	5.18	5.13	6.1
Eu	2.88		3.84	3.55	4.08	1.70	1.69	1.67	1.64	2.05
Tb	1.06		1.47	1.33	1.71	0.75	0.70	0.66	0.61	0.90
Yb	1.97		1.93	2.18	2.94	0.95	0.95	1.02	1.02	1.98
Lu	0.27		0.255	0.32	0.40	0.136	0.139	0.146	0.132	0.282
Cs	–		1.9	0.3	0.37	0.24	0.28	0.21	0.27	

[a] BHVO-1 data for ME and TE determined by XRF are from *Rhodes* [1996] and for TE determined by INAA are from *Ila and Frey* [2000]; in each case the same analytical methods were used for analysis of KERIMIS samples.

alkalic-tholeiitic dividing line [*MacDonald and Katsura*, 1964] in a total alkalis (Na_2O + K_2O) versus SiO_2 plot (Figure 5), whereas olivine basalts (D5) are clearly alkalic and plot in the field of the Lower Miocene basalts of the Kerguelen Archipelago [*Weis et al.*, 1993; *Frey et al.*, 2000b]. However, the whole rock compositions of the picritic basalts do not represent melt compositions as they have accumulated substantial amounts of olivine. Figure 6 shows the whole rock Mg # of Kerimis samples plotted against the forsterite (Fo) content of olivine phenocrysts and the Mg # of clinopyroxene phenocrysts. The whole rock Mg # were calculated assuming 10% Fe^{3+}, which corresponds to low-pressure crystallization conditions for oxygen fugacity of ~FMQ-1. The whole rock Mg # for the picritic basalts (D6) are too high for the measured olivine phenocryst compositions, based on an Fe/Mg

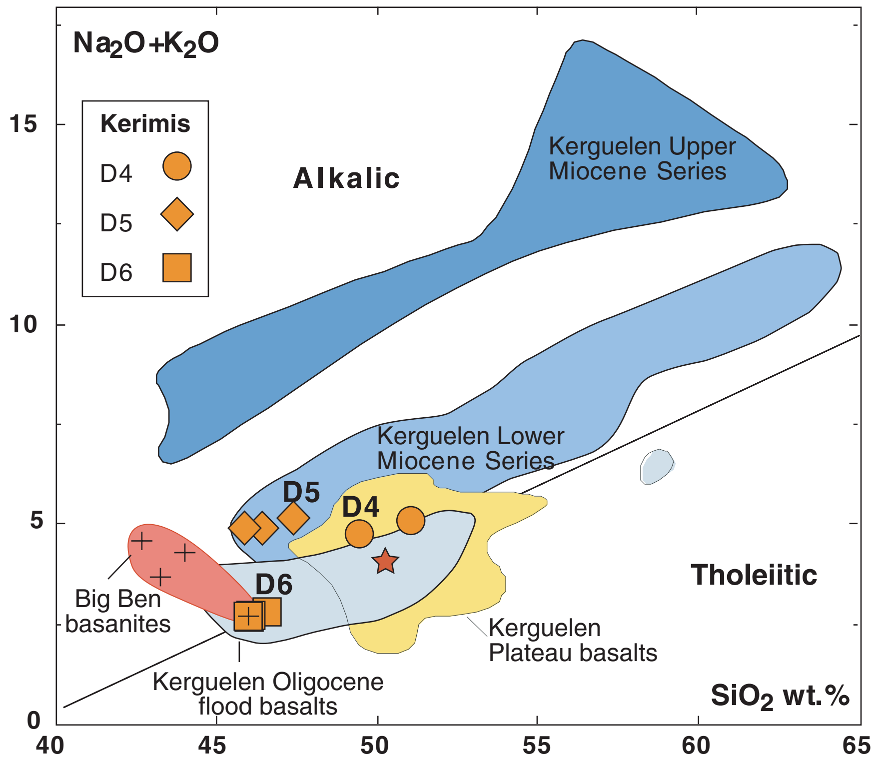

Figure 5. Total alkalis ($Na_2O + K_2O$) versus SiO_2 (all in wt %) classification plot. The star corresponds to D6 lava after correction for olivine addition. Shown for comparison are fields for different ages of lavas in the Kerguelen Archipelago, data for Cretaceous lavas from the Kerguelen Plateau and data (+) for basanites from Big Ben Volcano on Heard Island. Data Sources: Kerguelen Archipelago [*Weis et al.*, 1993; *Yang et al.*, 1998; *Frey et al.*, 2000b; unpublished manuscript, 1996]; Heard Island: [*Barling et al.*, 1994]; Kerguelen Plateau: [*Davies et al.*, 1989; *Mahoney et al.*, 1995].

exchange partition coefficient between olivine and basaltic liquid of 0.30 ± 0.03 [*Roeder and Emslie*, 1970], which indicates accumulation of $\sim Fo_{84}$ olivine in a basaltic melt with an Mg # of ~62. The equilibrium magma compositions for the picritic basalts were calculated by removing wt % increments of average olivine core compositions from the whole rock analysis for each sample until Fe/Mg equilibrium was attained. The results are coherent for each of the four samples and indicate an average equilibrium magma composition that contains ~6 vol % olivine phenocrysts, with a whole rock Mg # of 62 and MgO content of 8.5 wt %. The corrected average picritic basalt composition is shown in the total alkalis versus SiO_2 plot (Figure 5) and plots along the alkalic-tholeiitic dividing line (as predicted by simply removing olivine), but at significantly higher SiO_2 contents, ~50 wt %. Systematic removal of olivine phenocrysts also results in a more meaningful relationship between the whole rock Mg # and the Mg # of the ~1 vol % clinopyroxene phenocrysts in the picritic basalts; after correction, all of the clinopyroxene phenocrysts plot within the Fe/Mg equilibrium field (Figure 6b).

[29] The alkalic affinity of the D5 olivine basalts is also reflected in their abundances of incompatible elements, such as TiO_2, P_2O_5, and Nb, at a given MgO content (Figure 7). The olivine basalts (D5) are more enriched in incompatible elements than the lower Miocene alkalic basalts and the transitional Oligocene flood basalts of the Kerguelen Archipelago [*Yang et al.*, 1998; Frey, unpublished manuscript, 1996]. Their TiO_2 and P_2O_5 contents are most similar to the incompatible element-rich Upper Miocene basanites erupted in the southeast Province of the Kerguelen Archipelago [*Weis et al.*, 1993]. Surprisingly, the two D4 basalts of very different age (Table 2) are similar in composition (Table 3). Their compositions overlap with the

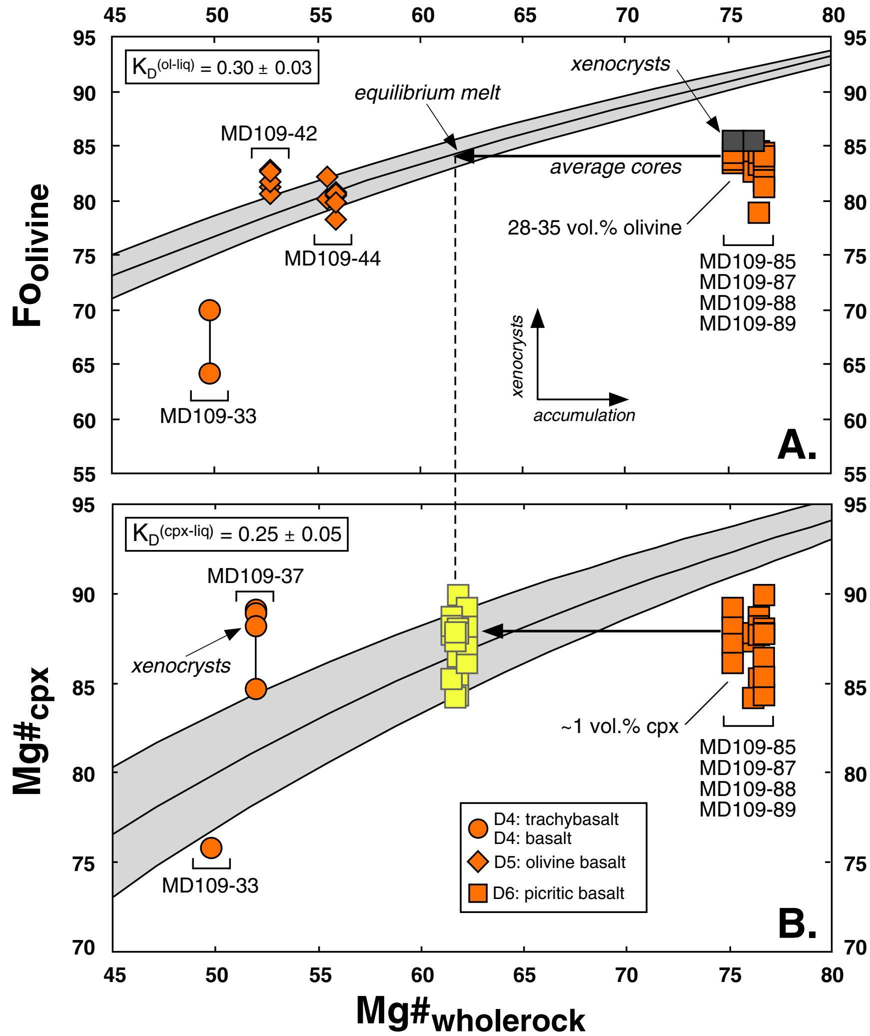

Figure 6. Plot of wholerock Mg #, where Mg # = (Mg/(Mg+Fe^{2+}))*100, versus the forsterite content of olivine (A) and the Mg # of clinopyroxene (B) for basaltic lavas from the Kerimis dredges. A. The gray field indicates the equilibrium field calculated using an Fe/Mg exchange partition coefficient between olivine and basaltic liquid of 0.30 ± 0.03 [*Roeder and Emslie*, 1970]. Note that the olivine xenocrysts from the D6 picritic basalts have slightly higher Fo contents than the phenocrysts. Olivine phenocrysts from the D5 olivine basalts are in equilibrium (MD109-44) or nearly in equilibrium (MD109-42) with their wholerock Mg #, whereas olivine microphenocrysts from the DR4 trachybasalt (MD109-33) fall well below the equilibrium field. B. The gray field indicates the equilibrium field calculated using an Fe/Mg exchange partition coefficient between clinopyroxene and basaltic liquid of 0.25 ± 0.05 [*Grove et al.*, 1982]. Recalculating the wholerock Mg # after olivine removal shows that all of the clinopyroxene phenocrysts from the picritic basalts plot in the equilibrium field.

fields of the flood basalts erupted in the Kerguelen Archipelago (Figures 5 and 7).

[30] Lavas associated with the Kerguelen mantle plume reveal a long-term systematic variation in Zr/Nb. Older lavas, 115 to 30 Ma, have Zr/Nb > 10, whereas <30 Ma lavas typically have Zr/Nb < 10 (Figure 8). The dredged lavas are consistent with this temporal trend; basalts (D4) and picritic basalts (D6) have higher Zr/Nb than olivine basalts (D5), but all of the dredged lavas have Zr/Nb < 10 (Figure 8). Lavas on the Kerguelen Archipelago show a long-term trend of increasing La/Yb with decreasing eruption age [*Frey et al.*, 2000b]. Consistent with this trend, the olivine and picritic basalts have high La/Yb, 25–20, within the range

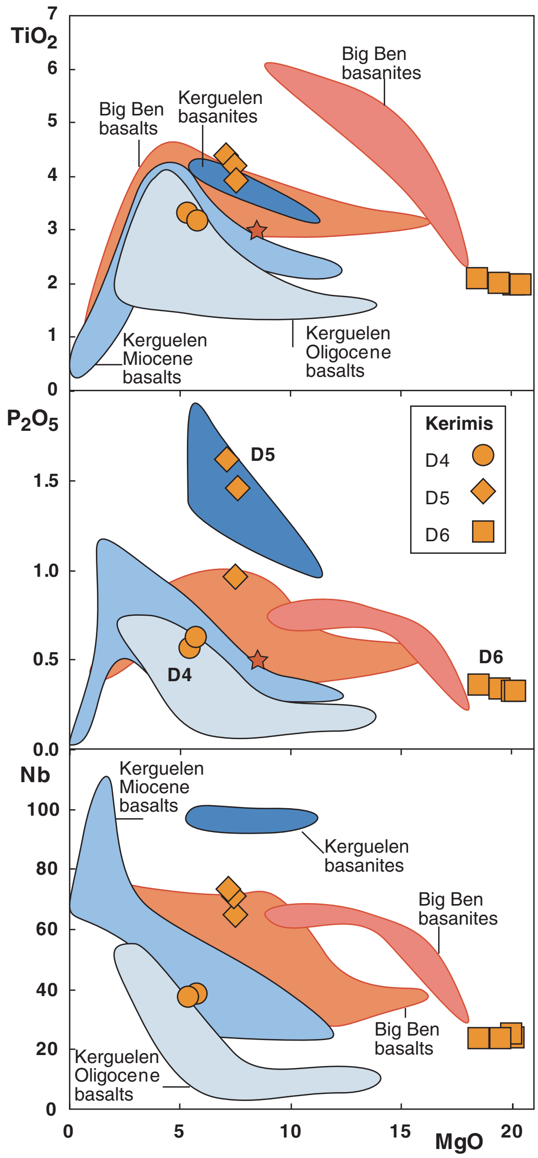

Figure 7. TiO_2, P_2O_5, and Nb versus MgO (oxides in wt % and Nb in ppm) in lavas forming the Kerguelen Archipelago and Heard Island. The incompatible element-rich D5 olivine basalts are most similar, but not identical, to basanites erupted during the upper Miocene in the Kerguelen Archipelago. The D6 picritic basalts are most similar to the high-MgO end of the recent Big Ben basanite sub-group erupted on Heard Island. Corrected for olivine addition (star), they overlap the Big-Ben basalt field and plot at the low P_2O_5 and TiO_2 end of the D5 olivine basalt trend. Data sources given in caption are the same as for Figure 5.

of lower Miocene basalts; a D4 basalt, however, has much lower La/Yb of 15 (Figure 8). The two main lava series on Heard Island (Laurens Peninsula and Big Ben) have different Ba/Nb ratios. These differences correlate with differences in Sr

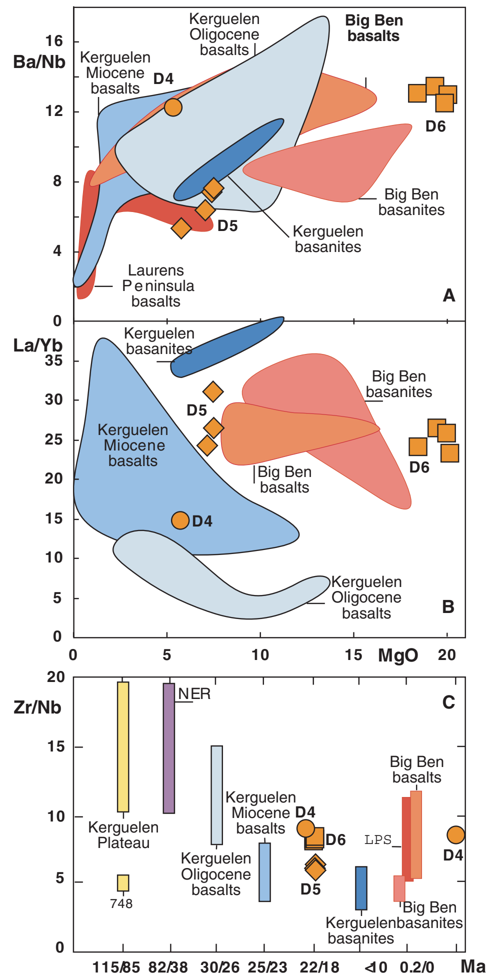

Figure 8. Ba/Nb (A) and La/Yb (B) versus MgO (wt %) and Zr/Nb versus eruption age for lavas associated with the Kerguelen plume (C). In panel A, which distinguishes the two main lava series on Heard Island (Laurens Peninsula, LPS and Big Ben, BBS), the picrites (D6) overlap with the BBS and the D5 lavas overlap with the LPS. Data sources as for Figure 5. In panel B, the La/Yb of the basalt (D4) and of olivine lavas (D5) are in the range of Miocene alkalic flood basalts of the Kerguelen Archipelago. The picrites have similar La/Yb, and plot near the MgO-rich end of the Big Ben basanite field. In the bottom panel C, the time axis is not linear. The Cretaceous lavas drilled from the Kerguelen Plateau and Ninetyeast Ridge are tholeiitic basalts with relatively high Zr/Nb, with the exception of ODP Site 748 where they are alkalic [*Storey et al.*, 1992; *Frey et al.*, 1991]. The Oligocene flood basalts from the Kerguelen Archipelago have transitional major element compositions with intermediate Zr/Nb ratios [*Yang et al.*, 1998] whereas the alkalic Miocene flood basalts from the Kerguelen Archipelago have lower Zr/Nb [*Frey et al.*, 2000b]. The Kerimis dredged lavas have Zr/Nb similar to the latter as well as to the recent alkalic lavas erupted in the Kerguelen Archipelago and Heard Island.

Table 4. Isotopic Ratios for the Kerimis Dredged Basalts

Dredges	Samples	$^{87}Sr/^{86}Sr$	$2\sigma_m$	$^{143}Nd/^{144}Nd$	$2\sigma_m$	$^{206}Pb/^{204}Pb^a$	$^{207}Pb/^{204}Pb^a$	$^{208}Pb/^{204}Pb^a$	$^{176}Hf/^{177}Hf$	$2\sigma_m$
4	33	0.703126	6	0.512946	14	19.669	15.678	39.315	0.282937	8
	33[b]	0.703100	6	0.512942	9	19.677	15.686	39.347		
4	37	0.705942	6	0.512525	9	18.451	15.551	39.009		
5	42	0.705654	6	0.512582	10	18.179	15.511	38.576		
5	44a	0.705625	7	0.512606	8	18.214	15.517	38.634	0.282752	8
5	44b	0.705658	8	0.512576	10	18.208	15.527	38.658		
		0.705676	11			18.197	15.524	38.662		
6	85	0.705694	8	0.512543	8	17.875	15.536	38.266		
6	87	0.705683	10	0.512533	6	17.874	15.540	38.274		
6	88	0.705681	8	0.512547	7	17.872	15.538	38.265	0.282728	7
		0.705703	7			17.869	15.531	38.266		
6	89	0.705699	6	0.512526	9	17.876	15.541	38.278		
		0.705683	12							

[a] Absolute $2\sigma_m$ errors for the Pb isotopic analysis are between 0.015 and 0.017 for $^{206}Pb/^{204}Pb$ and $^{207}Pb/^{204}Pb$ and between 0.045 and 0.050 for $^{208}Pb/^{204}Pb$.
[b] Full-procedural duplicate analysis, including leaching.

and Nd isotopic ratios, and the high Ba/Nb ratios are inferred to be derived from a continental crust component [*Barling et al.*, 1994]. Olivine basalts (D5) have relatively low Ba/Nb within the range of the Laurens Peninsula series, but basalts (D4) and picritic basalts (D6) overlap with the Big Ben series and the Oligocene to Miocene flood basalts forming the Kerguelen Archipelago (Figure 8).

[31] In summary, the major and trace element abundances of lavas from each dredge form distinct compositional groups (Figures 5, 7, and 8). The basalts (D4) have the lowest abundances of incompatible elements; they are similar in composition to flood basalts erupted in the Kerguelen Archipelago. In contrast, D5 olivine basalts have significantly higher abundances of incompatible elements, exceeding those of the Kerguelen Archipelago flood basalts and approaching those of basanites erupted in the Kerguelen Archipelago and at Heard Island. The D6 picritic basalts are not typical of lavas associated with the Kerguelen plume; these picrites are most similar to the MgO-rich lavas of the Big Ben basanitic series erupted on Heard Island.

3.4. Isotope Ratios

[32] All isotope ratios are reported in Table 4.

3.4.1. Sr-Nd-Hf-Pb isotopic variations

[33] In a Sr-Nd diagram (Figure 9), all the 18–21 Ma basalts (i.e., the olivine basalts (D5), the picritic pillow basalts (D6) and the alkali basalt (D4)) plot within the field defined by the Upper Miocene Series of the Kerguelen Archipelago [*Weis et al.*, 1993]. The effect of age-correction for in situ ^{87}Rb and ^{147}Sm decay is negligible (between 3 and 5 $\times$ 10^{-5} and 1.1 and 1.5 $\times$ 10^{-5}, respectively). D6 picritic basalts have slightly lower $^{143}Nd/^{144}Nd$ than D5 alkali basalts and plot within the field of the archipelago basanites. More than 90% of the Kerguelen Archipelago Miocene flood basalts have $^{87}Sr/^{86}Sr$ between 0.7050 and 0.7056 and $^{143}Nd/^{144}Nd$ between 0.5127 and 0.5125, while the Oligocene flood basalts present a larger range, extending toward more depleted isotopic compositions [*Weis et al.*, 1998a; *Yang et al.*, 1998]. Surprisingly, the slightly alkalic, younger D4 basalt which was analyzed in duplicate (sample D4-33) plots within the field defined by the depleted basalts of MORB from the southeast Indian Ridge. This sample is similar in composition to D4-37 (Table 3).

[34] In contrast to the relatively homogeneous Sr-Nd isotopic compositions, alkali (D4) and olivine (D5) basalts and picritic basalts (D6) have distinct Pb isotopic ratios (Figure 10). The D5 olivine basalts plot within the less radiogenic part of the field defined by the Kerguelen Archipelago Oligocene flood basalts [*Yang et al.*, 1998]. They have slightly lower $^{207}Pb/^{204}Pb$ than lavas from Heard Island and the youngest lavas from the Kerguelen Archipelago, the Upper Miocene Series and basan-

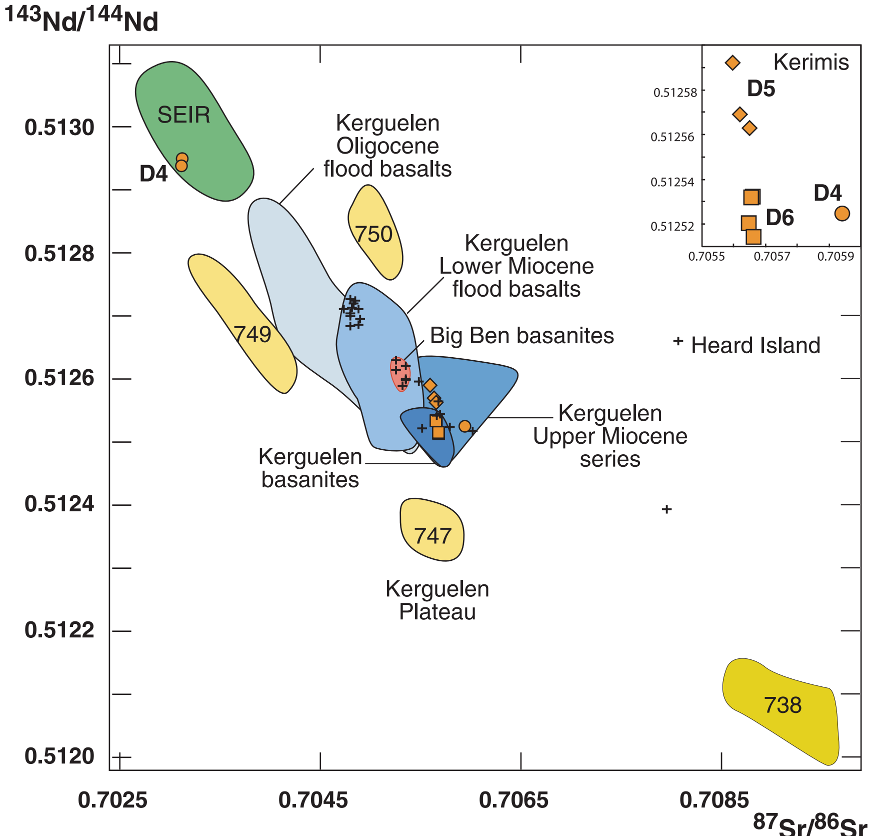

Figure 9. $^{87}Sr/^{86}Sr - ^{143}Nd/^{144}Nd$. Isotope plots for Kerimis dredged basalts compared with fields for Kerguelen Archipelago and Kerguelen Plateau basalt fields as well as other volcanic features of the Indian Ocean. Data sources as in Figures 5 and 8, plus: Southeast Indian Ridge (SEIR): [*Hamelin et al.*, 1985/1986; *Michard et al.*, 1986; *Price et al.*, 1986; *Dosso et al.*, 1988; *Mahoney et al.*, 1998]. Olivine and picritic basalts (D5, D6) have comparable $^{87}Sr/^{86}Sr$ but distinct $^{143}Nd/^{144}Nd$ with the olivine basalts being slightly less radiogenic (see detailed inset). All Kerguelen Plateau basalts as well as Kerguelen Archipelago flood basalts have been corrected for in situ ^{87}Rb and ^{147}Sm decay since their emplacement age.

ites of the southeast Province [*Weis et al.*, 1993] and lavas from Mount Ross [*Weis et al.*, 1998b]. Relative to the picritic basalts (D6), the olivine basalts (D5) have lower $^{207}Pb/^{204}Pb$ and higher $^{143}Nd/^{144}Nd$. The D6 picritic basalts have very homogeneous Pb isotopic ratios, distinctly less radiogenic than those of the Kerguelen Archipelago basalts, but they overlap with the Pb isotopic ratios in dredged and drilled basalts from the Kerguelen Plateau [*Weis et al.*, 1989a; *Mahoney et al.*, 1995], as well as the least radiogenic end of the Heard Island trend [*Barling et al.*, 1994].

[35] The two alkali basalts from D4 have very different Pb isotopic compositions (Figure 10). Sample D4-33 has very radiogenic Pb isotopic compositions falling in the field defined by the Comores Archipelago [*Class and Goldstein*, 1997], whereas sample D4-37 plots within the field of Kerguelen Archipelago Miocene flood basalts (Figure 10).

[36] The Hf isotopic composition of three basalts was determined, one from each dredge, in order to compare with basalts from the Kerguelen Archipelago and the Kerguelen Plateau [*Mattielli et al.*, 2000]. The olivine (D5) and the picritic (D6) basalts have very comparable Hf isotopic ratios, while sample D4-33, because of its higher $^{206}Pb/^{204}Pb$, again plots within the range of Comores basalts [*Salters and White*, 1998].

3.4.2. He isotopes

[37] Helium isotopic ratios have been used as a geochemical tracer to identify magmas derived

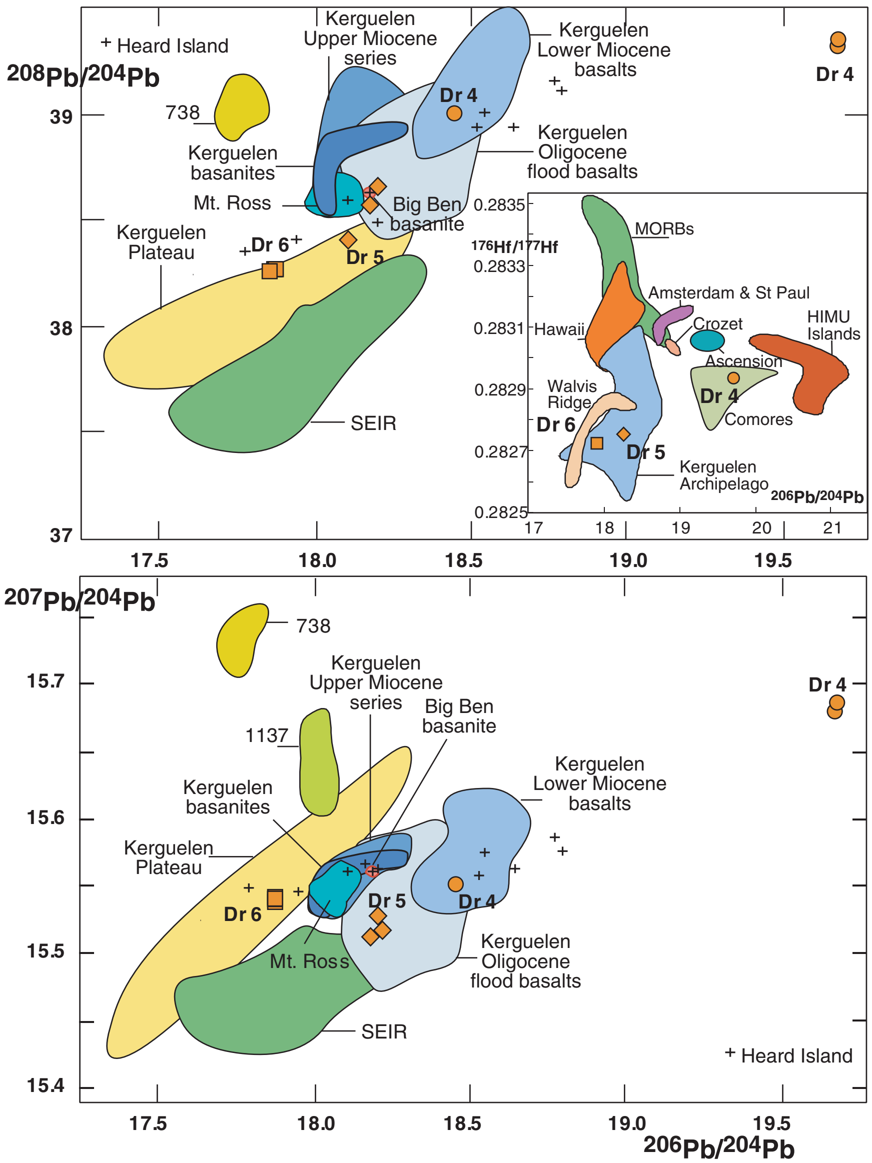

Figure 10. $^{207}Pb/^{204}Pb - ^{206}Pb/^{204}Pb$ and $^{208}Pb/^{204}Pb - ^{206}Pb/^{204}Pb$. Data sources as in Figure 9, plus Site 1137 [*Weis et al.*, 2001]. Pb isotope compositions discriminate between the various Kerimis dredge sites. The inset reports $^{176}Hf/^{177}Hf - ^{206}Pb/^{204}Pb$ and comparison with literature data [*Salters and White*, 1998].

from relatively undegassed mantle [e.g., *Kurz et al.*, 1983; *Condomines et al.*, 1983; *Graham et al.*, 1999]. Because of the relatively rare occurrence of olivine phenocrysts, very few samples from the Kerguelen mantle plume environment have been analyzed for $^3He/^4He$; the exception is Heard Island [*Hilton et al.*, 1995] where basanites and other MgO-rich lavas are much more common. A dredged picritic basalt (D6-88) was analyzed for its He isotopic compositions and yields a $^3He/^4He$ of 8.8 ± 0.5 R/R_A (1σ), where R/R_A is the $^3He/^4He$ ratio of the sample relative to an atmospheric $^3He/^4He$ of 1.39×10^{-6}. This value is more typical of southeast Indian Ridge basalts (7.73–9.70 R/R_A [*Graham et al.*, 1999]) than of higher $^3He/^4He$ ocean island basalts interpreted to have an undegassed mantle component [e.g., *Kurz and Jenkins*, 1981; *Kurz et al.*, 1982; *Poreda et al.*, 1986]. However, previous and ongoing studies show that the Kerguelen Archipelago lavas generally have low $^3He/^4He$ ratios (4.9– 10.2 R/R_A; [*Vance et al.*, 1989; *Nicolaysen et al.*, 1998]) as do lavas of the Big Ben Series on Heard (3.9–8.4 R/R_A [*Hilton et al.*, 1995]). In contrast, olivines from Laurens Peninsula lavas on Heard Island give R/R_A at 18.1, which *Hilton et al.* [1995] considered as representative of the Kerguelen plume helium isotopic signature.

4. Discussion

4.1. Source Characteristics of Dredged Lavas on the Seamounts

[38] Recent stratigraphic studies of volcanic sections on the Kerguelen Archipelago indicate that the isotopic composition of the Kerguelen mantle plume is best represented by the 24 Ma mildly alkalic basalts from the Mt. Crozier section that have the most radiogenic Pb isotopic compositions [e.g., *Weis et al.*, 1998a]. Younger lavas from the Upper Miocene series or the Ross volcano [*Weis et al.*, 1993, 1998b] have distinctly lower $^{206}Pb/^{204}Pb$ ratios pointing towards the Kerguelen Plateau, while the Oligocene flood basalts, 29–25 Ma, have isotopic compositions indicative of interaction with the depleted mantle [*Gautier et al.*, 1990; *Yang et al.*, 1998; *Weis et al.*, 1998a]. Except for sample D4-33, all Sr, Nd, and Hf isotopic ratios for the seamount basalts overlap the field of Kerguelen Archipelago lavas (Figure 9) and indicate an origin by partial melting of the Kerguelen mantle plume. The Pb ratios in the picritic basalts (D6), however, extend toward lower $^{206}Pb/^{204}Pb$ or higher $^{207}Pb/^{204}Pb$ and $^{208}Pb/^{204}Pb$ for a given $^{206}Pb/^{204}Pb$, i.e., toward the field for Kerguelen Plateau lavas. In the extreme case of ODP Site 738 on the southern Kerguelen Plateau and of Elan Bank at ODP Site 1137 (Figure 10), the Pb isotope characteristics are indicative of incorporation of continental lithosphere by the ascending magma derived from the Kerguelen plume [*Mahoney et al.*, 1995; *Frey et al.*, 2000a; *Weis et al.*, 2001]. None of the dredged samples from between the Kerguelen Archipelago and Heard Island have the extreme isotopic characteristics of Site 738 basalts, which include very high $^{87}Sr/^{86}Sr$, low $^{143}Nd/^{144}Nd$ and very high $^{207}Pb/^{204}Pb$ and $^{208}Pb/^{204}Pb$ for a given $^{206}Pb/^{204}Pb$ (Figures 9 and 10), or those of Site 1137 basalts from Elan Bank that reflect increasing upper crust contamination with age [*Ingle et al.*, 2000; *Weis et al.*, 2001]. The lavas erupted on Heard Island show a distinctly larger range of isotopic compositions [*Barling et al.*, 1994] than those erupted on the Kerguelen Archipelago, ranging to higher $^{87}Sr/^{86}Sr$ and lower $^{143}Nd/^{144}Nd$ and from high $^{206}Pb/^{204}Pb$ to the relatively low $^{206}Pb/^{204}Pb$, typical of the Kerguelen Plateau basalts (Figures 9 and 10).

[39] If the low $^{143}Nd/^{144}Nd$ and $^{206}Pb/^{204}Pb$ of some Kerguelen Plateau lavas can be attributed to a continental component, then the D6 picrites and some Heard Island lavas may contain some of this component, which is not present in the D5 olivine basalts nor in most of Kerguelen Archipelago basalts. The abundance ratio La/Nb has also been used to identify a continental component in lavas associated with the Kerguelen plume [*Mahoney et al.*, 1995; *Coffin et al.*, 2000]. None of these dredged samples are depleted in Nb. For example La/Nb varies from 0.84 to 0.97 and 0.99 to 1.03 in D5 and D6 lavas, respectively, compared to the primitive mantle estimate of 0.96 [*Sun and McDonough*, 1989]. The low $^{143}Nd/^{144}Nd$ and $^{206}Pb/^{204}Pb$ in D6 picrites may reflect interaction of the plume-derived magmas with the Cretaceous Kerguelen Plateau, but there is no compelling compositional evidence for a component derived from continental crust. The modest helium isotopic ratio ($^3He/^4He$ = 8.8 R/R_A) of D6-88 may indicate that the picrites do not represent pristine plume melts. In the case of Heard Island where a wide range in $^3He/^4He$ (∼5 to 18 R_A) occurs in lavas from a single island, *Hilton et al.* [1995] interpreted the low He R/R_A values as reflecting shallow-level contamination by radiogenic He.

[40] One, apparently <1 Ma, alkali basalt sample, D4-33, has a chemical composition similar to those of the Lower Miocene flood basalts of the Kerguelen Archipelago, but its isotopic compositions are MORB-like for Sr-Nd, while its Pb composition plots within the field defined by lavas from the Comores, another Indian Ocean Island, situated more than 4600 km to the west. Currently, we have

no explanation for the puzzling isotopic characteristics or for the age of this sample.

4.2. Kerguelen Hot Spot Track

[41] The exact location of the Kerguelen hot spot has long been a matter of debate. In tectonic reconstructions of the Indian Ocean basin, *Müller et al.* [1993], amongst others, required that the present location of the Kerguelen hot spot be beneath Skiff Bank, under the northwestern Northern Kerguelen Plateau, in order to acceptably model the location fit of Ninetyeast Ridge using a fixed hot spot reference frame. *Steinberger* [2000] assumed a present location under the Kerguelen Archipelago, which improves the fit of Ninetyeast Ridge and the Rajmahal traps when compared to results from fixed hot spot models. According to *Steinberger* [2000], none of the mantle models gives an acceptable fit of Ninetyeast Ridge and the Rajmahal traps if the present location of the Kerguelen hot spot is assumed to be under Heard Island. All models nevertheless agree in predicting a southward surface motion for the Kerguelen hot spot.

[42] Recent argon dating from ODP Site 1139 (Leg 183) clearly rules out Skiff Bank (∼68 Ma [*Duncan and Pringle*, 2000]) as the current location of the Kerguelen hot spot. More recent volcanic activity on the Kerguelen Archipelago and Heard Island leave them more viable candidates for the location of the hot spot.

[43] The age range of 21–18 Ma for the seamounts between the Kerguelen Archipelago and Heard Island is slightly younger than the main peak of volcanism on the Kerguelen Archipelago and intermediate between the peak of the volcanism on these two main islands. Although they are more enriched in incompatible elements, the D5 alkali basalts are similar in major element composition to the 24–25 Ma Miocene alkalic flood basalts in the eastern part of the Kerguelen Archipelago and the D6 picrites are most similar to the high-MgO Big Ben basanites erupted on Heard Island. The geochemical and isotopic similarities of D5 and D6 lavas with Miocene to recent alkaline lavas erupted in the Kerguelen Archipelago and Heard Island indicate comparable sources for these lavas. Given the evidence for a common source and the spatial variations in age and volume of magmatism (Figure 11), it is possible that the trend from ODP Site 1140 through the Kerguelen Archipelago to the dredged submarine volcanoes, and even possibly to Heard and McDonald Islands, corresponds to the hot spot track of the Kerguelen plume.

[44] Another possibility is that the Miocene to Recent volcanism associated with the Kerguelen plume has become more diffuse because the plume is beneath the thick Kerguelen Plateau. In this case, definitive identification of the current location of the plume may be beyond our grasp. The thick Cretaceous lithosphere may have limited decompressional melting and forced melts to exploit lithosphere weaknesses for ascent and eruption [*Barling et al.*, 1994]. Three observations consistent with this interpretation are as follows: (1) the numerous mantle xenoliths in the alkalic lavas of the Kerguelen Archipelago which require rapid transport and exploitation of lithospheric fractures [*Grégoire et al.*, 1998]. (2) Despite this evidence for rapid transport of mafic lavas, the trachytes, phonolites, and other evolved lavas erupted in the Kerguelen Archipelago and at Heard and McDonald Islands demonstrate that some magmas stagnated and fractionated within the lithosphere. (3) With decreasing eruption age in the Kerguelen Archipelago, lavas with similar Sr and Nd isotopic ratios increase in La/Yb (Figure 8). This trend is consistent with a temporal decrease in extent of melting and increase in depth of melt segregation.

5. Conclusions

[45] The seamounts dredged between the Kerguelen Archipelago and Heard Island during the recent Kerimis survey cruise, in the Northern (previously unsampled) and Central Kerguelen Plateau, are formed by Miocene mildly alkalic basalts and picrites. The latter are the first discovered picritic basalts related to the Kerguelen plume activity.

[46] The alkalic compositional characteristics of the dredged basalts are consistent with the temporal

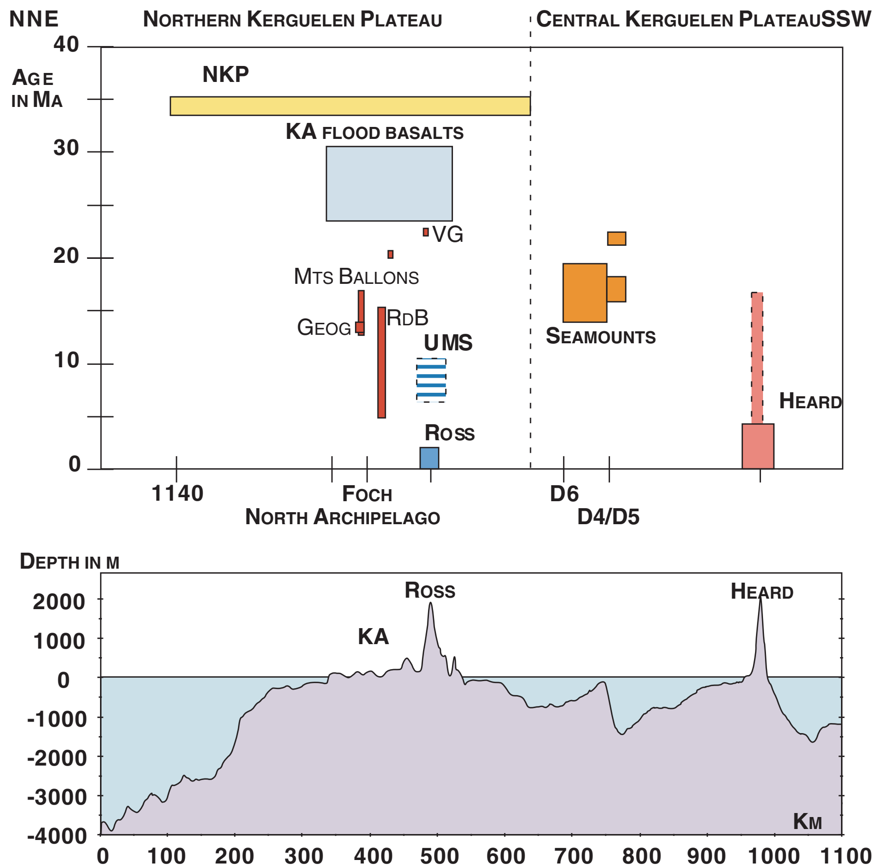

Figure 11. Plot showing the relative position of magmatic products related to the Kerguelen mantle plume versus their age. Age data are from *Duncan and Pringle* [2000] for ODP Site 140 in the NKP, from *Nicolaysen et al.* [2000] for Kerguelen Archipelago flood basalts, from *Weis and Giret* [1994] for the Kerguelen Archipelago plutonic complexes (in italics) and from *Clarke et al.* [1983] and *Quilty et al.* [1983] for Heard Island. The relative distance is calculated along two straight lines (see Figure 2) along which the bathymetric profiles (bottom part) have also been drawn, one from ODP Site 1140 to the Mt. Ross volcano on the Kerguelen Archipelago and the other one from the Mt. Ross volcano to Heard Island, passing through the dredged seamount. This plot shows clearly the southwards migration with time of the location of the most voluminous emissions of basaltic magma related to the Kerguelen plume, as the volume of magma associated with the seamounts and Heard Island greatly exceeds that of the relatively small volcano-plutonic complexes on the Kerguelen Archipelago (Val Gabbro (VG), Mts Ballons, Rallier du Baty (RdB), Géographie) and of the basanite to phonolite plugs and domes of the Upper Miocene Series (UMS).

trends of Kerguelen plume magmatism, from >25 Ma tholeiitic/transitional basalts to <25 Ma alkalic basalts, a trend that probably reflects a decrease in degree of mantle melting [*Weis et al.*, 1998b; *Frey et al.*, 2000b]. Olivine and picritic basalts from D5 and D6 have Sr-Nd isotopic compositions within the range defined by >90% of the Kerguelen Archipelago Miocene flood basalts and the Big Ben basaltic series on Heard Island suggesting that these lavas have been produced by partial melting of the Kerguelen plume. D5 and D6 basalts have distinct Pb isotopic compositions for comparable Sr isotopic ratios. D5 olivine basalts have Pb ratios comparable to those of the Kerguelen Archipelago Oligocene lavas, whereas D6 picritic basalts have Pb ratios plotting within the field of Kerguelen Plateau basalts, which are characterized by lower $^{206}Pb/^{204}Pb$ values. One D4 alkali basalt, sample D4-33, is unique in its isotopic ratios in the context of the Kerguelen plume magmatism; it has MORB-

Table A1. Representative Electronprobe Analyses of Olivine From Kerimis MD109 Basalts [The full Appendix A1 is available in the HTML version of the article at http://www.g-cubed.org.]

Dredge	D4		D5											
Sample	MD109-33		MD109-42		MD109-44a					MD109-44b				
Rock type[a]	TB		B		B					B				
Type[b]	Phen.	Mic.	Phen.	Phen.	Phen.	Phen.	Phen.	Phen.	Phen.	Phen.	Phen.	Phen.	Phen.	Phen.
Kind[c]	E	S	SK	S	SK	E	S	SK	E	SK	SK	SK	E	E
Oxides (wt %)														
SiO_2	37.75	36.34	38.88	39.32	39.42	39.41	39.11	38.70	38.69	39.06	38.35	38.71	38.64	38.55
Cr_2O_3	0.12	0.00	0.01	0.04	0.05	0.03	0.01	0.02	0.04	0.00	0.05	0.00	0.01	0.03
FeO	26.98	35.29	18.53	16.68	17.87	18.16	18.11	20.14	18.64	16.22	17.85	17.10	17.35	16.33
MnO	0.30	0.48	0.18	0.25	0.25	0.19	0.19	0.23	0.25	0.19	0.20	0.18	0.17	0.24
MgO	35.51	28.60	42.63	44.05	42.92	42.92	42.74	41.42	42.17	43.98	42.35	43.71	43.15	44.62
CaO	0.17	0.17	0.26	0.25	0.24	0.16	0.23	0.31	0.22	0.16	0.21	0.23	0.25	0.15
NiO	0.10	0.08	0.27	0.28	0.18	0.16	0.16	0.17	0.16	0.30	0.15	0.26	0.24	0.29
Total	100.98	101.03	100.91	100.87	100.95	101.03	100.59	101.10	100.28	99.96	99.20	100.22	99.90	100.22
Cations (pfu.)														
Si	0.995	0.999	0.986	0.989	0.995	0.994	0.992	0.987	0.988	0.990	0.987	0.983	0.985	0.976
Cr	0.002	0.000	0.000	0.001	0.001	0.001	0.000	0.000	0.001	0.000	0.001	0.000	0.000	0.001
Fe^{2+}	0.595	0.811	0.393	0.351	0.377	0.383	0.384	0.430	0.398	0.344	0.384	0.363	0.370	0.346
Mn	0.007	0.011	0.004	0.005	0.005	0.004	0.004	0.005	0.005	0.004	0.004	0.004	0.004	0.005
Mg	1.396	1.172	1.612	1.652	1.615	1.615	1.616	1.575	1.606	1.661	1.625	1.655	1.640	1.685
Ca	0.005	0.005	0.007	0.007	0.007	0.004	0.006	0.008	0.006	0.004	0.006	0.006	0.007	0.004
Ni	0.002	0.002	0.006	0.006	0.004	0.003	0.003	0.003	0.003	0.006	0.003	0.005	0.005	0.006
Sum	3.003	3.000	3.011	3.010	3.004	3.005	3.007	3.011	3.010	3.009	3.011	3.017	3.013	3.023
End members (%)														
Fo	70.0	58.9	80.1	82.2	80.8	80.6	80.5	78.2	79.9	82.7	80.7	81.8	81.3	82.8
Fa	30.0	41.1	19.9	17.8	19.2	19.4	19.5	21.8	20.1	17.3	19.3	18.2	18.7	17.2

[a] Rock type: PB, picritic basalt; B, basalt; TB, trachybasalt.
[b] Grain size: Phen. and Xen., pheno/xenocrysts > 0.7 mm; Mic., microphenocrysts > 0.3 mm; Glom., glomerocryst > 0.7 mm.
[c] Phenocryst morphology: E, euhedral; S, subhedral; A, anhedral; SK, skeletal; R, rounded.

Table A2. Representative Electronprobe Analyses of Clinopyroxene From Kerimis MD109 Basalts

Unit	D4				D6		D6				D6		D6			
Sample Rock type[a]	MD109-37 B				MD109-85 PB		MD109-87 PB				MD109-88 PB		MD109-89 PB			
Type[b] Kind[c]	Phen. E		Xen. S		Phen. E		Phen. E		Phen. E		Phen. R		Phen. E		Phen. E	
Zone	core	Rim	core	rim	core	rim	core	rim	core	rim	core	rim	core	mid	core	rim
Oxides (wt. %)																
SiO_2	51.24	46.23	51.33	52.19	49.55	50.99	51.03	51.22	52.13	50.63	51.53	52.19	52.20	51.68	52.40	52.31
TiO_2	1.29	2.97	0.82	0.90	1.58	1.09	0.93	1.14	0.81	1.26	0.96	1.01	0.90	1.24	0.80	0.89
Al_2O_3	2.60	6.26	2.40	2.60	3.47	1.71	1.72	2.38	2.07	2.73	2.44	2.49	1.91	2.44	1.82	1.88
Cr_2O_3	0.04	0.15	0.75	0.81	0.23	0.44	0.17	0.43	0.72	0.51	0.92	0.84	0.67	0.25	0.93	0.79
FeO_{tot}	7.21	8.75	5.96	5.67	6.23	5.92	5.84	5.57	4.97	5.82	5.11	5.44	4.50	6.28	4.43	4.66
MnO	0.14	0.19	0.14	0.01	0.11	0.05	0.14	0.07	0.13	0.08	0.09	0.13	0.06	0.14	0.03	0.07
MgO	16.06	13.68	17.66	17.36	15.56	17.20	16.21	16.50	16.82	16.42	16.37	16.49	17.14	16.47	16.82	16.84
CaO	21.55	21.09	20.55	20.47	21.51	20.96	22.36	21.47	21.65	21.57	22.11	21.98	22.45	21.44	22.02	21.67
Na_2O	0.31	0.36	0.35	0.34	0.31	0.17	0.25	0.24	0.26	0.20	0.26	0.30	0.27	0.35	0.20	0.26
Total	100.44	99.68	99.96	100.37	98.55	98.53	98.65	99.02	99.54	99.24	99.78	100.88	100.09	100.30	99.44	99.35
Cations (pfu.)																
Si	1.882	1.726	1.882	1.901	1.850	1.905	1.907	1.897	1.917	1.876	1.895	1.899	1.909	1.893	1.929	1.927
Al^{IV}	0.113	0.274	0.104	0.099	0.150	0.075	0.076	0.103	0.083	0.119	0.105	0.101	0.082	0.105	0.071	0.073
Al^{VI}	0.000	0.002	0.000	0.013	0.002	0.000	0.000	0.001	0.007	0.000	0.000	0.006	0.000	0.000	0.008	0.009
Cr	0.001	0.004	0.022	0.023	0.007	0.013	0.005	0.013	0.021	0.015	0.027	0.024	0.019	0.007	0.027	0.023
Fe^{3+}	0.062	0.127	0.062	0.037	0.075	0.013	0.037	0.044	0.029	0.048	0.043	0.037	0.032	0.055	0.007	0.011
Ti	0.036	0.083	0.023	0.025	0.044	0.031	0.026	0.032	0.022	0.035	0.027	0.028	0.025	0.034	0.022	0.025
Mg	0.879	0.762	0.965	0.943	0.866	0.958	0.903	0.911	0.922	0.907	0.897	0.894	0.934	0.899	0.923	0.924
Fe^{2+}	0.159	0.146	0.121	0.135	0.120	0.172	0.146	0.129	0.124	0.132	0.114	0.128	0.105	0.138	0.129	0.133
Mn	0.005	0.006	0.004	0.000	0.004	0.002	0.005	0.002	0.004	0.003	0.003	0.004	0.002	0.004	0.001	0.002
Ca	0.848	0.844	0.807	0.799	0.860	0.839	0.895	0.852	0.853	0.856	0.871	0.857	0.880	0.841	0.868	0.855
Na	0.022	0.026	0.025	0.024	0.022	0.012	0.018	0.017	0.018	0.014	0.018	0.021	0.019	0.025	0.015	0.019
Sum	4.006	4.000	4.014	4.000	4.000	4.020	4.017	4.000	4.000	4.005	4.000	4.000	4.008	4.002	4.000	4.000
End members (%)																
En	49.6	51.9	54.5	53.6	51.8	49.3	47.8	51.3	51.4	51.4	51.6	51.1	51.0	50.8	50.5	50.6
Fs	9.0	10.0	6.8	7.7	7.2	8.9	7.7	7.2	6.9	7.5	6.5	7.3	5.7	7.8	7.1	7.3
Wo	41.4	38.1	38.7	38.7	41.1	41.9	44.5	41.5	41.7	41.1	41.9	41.6	43.3	41.5	42.4	42.1
Mg#	84.7	83.9	88.9	87.5	87.8	84.8	86.1	87.6	88.1	87.3	88.724	87.476	89.9	86.7	87.7	87.4

[a] Rock type: PB, picritic basalt; B, basalt; TB, trachybasalt.
[b] Grain size: Phen., phenocrysts > 0.7 mm; Mic., microphenocrysts > 0.3 mm; Grain, groundmass < 0.3 mm.
[c] Phenocryst morphology: E, euhedral; S, subhedral; A, anhedral.

Table A3. Petrographic Characteristics of Samples From the Kerimis MD 109 Dredge Sites

		Rock Name[a]				Phenocrysts,[b] vol %					Phenocryst Sizes, mm		
Sample	Dredge	PB	B	TB	Vesicles, vol %	Ol	Cpx	Plag	Ox	**Total**	Ol	Cpx	Plag
MD109-33	4	–	–	X	8.3	3.8	0.9	8.7	–	**13.3**	1–2	1–2	1–5
MD109-37	4	–	X	–	–	2.3	3.7	2.7	–	**8.7**	0.7–3	1–4	0.7–1.5
MD109-42	5	–	X	–	–	6.9	–	–	–	**6.9**	0.5–2	–	–
MD109-44a	5	–	X	–	–	7.8	–	–	–	**7.8**	0.5–2	–	–
MD109-44b	5	–	X	–	–	7.3	–	–	–	**7.3**	0.5–2	–	–
MD109-85	6	X	–	–	–	34.2	1.0	–	0.6	**35.7**	2–5	~2	–
MD109-87	6	X	–	–	–	28.0	0.4	–	0.1	**28.4**	2–5	~2	–
MD109-88	6	X	–	–	–	30.4	1.3	–	0.1	**31.9**	2–5	~2	–
MD109-89	6	X	–	–	–	35.3	0.8	–	–	**36.1**	2–5	~2	–

[a] Rock names: picritic basalt (PB), basalt (B), and trachybasalt (TB).
[b] Phenocryst abundances were determined by point counting with 1500 points/slide.

like Sr and Nd ratios and high $^{206}Pb/^{204}Pb$, similar to lavas from the Comores Islands.

[47] The last 34 myr of mildly alkalic volcanism in the north central region of the Kerguelen Plateau has been spatially diverse with coeval volcanism on the Kerguelen Archipelago, at Heard and McDonald Islands, and at submarine structures between these islands. Although there has been coeval volcanism, there appears to be a general trend for recent volcanism to migrate in a southeasterly direction from the Northern Kerguelen Plateau to the Kerguelen Archipelago and finally to Heard and McDonald Islands. This trend may well represent the Tertiary hot spot track of the Kerguelen plume.

Acknowledgments

[48] The Kerimis program was supported by the Institut National des Sciences de l'Univers (INSU-CNRS) and by the Université Louis Pasteur (Ecole et Observatoire des Sciences de la Terre). The senior author of this paper thanks the FNRS for financing this research program (FRFC Grant 2.4579.99). D. Damasceno thanks the FRIA for financing his Ph.D. scholarship. Both Weis and Damasceno thank the FNRS for financing their participation in the Kerimis survey cruise. Part of this research program was also funded by the ARC convention 98/03-233. C. Maerschalk is thanked for carefully preparing the samples for isotope analyses and M. Lo Cascio for diligently crushing them. Research done at MIT was supported by NSF Grant EAR 98141313. We thank P. Ila (MIT) and M. Vollinger (University of Massachusetts) for obtaining INAA and XRF data, respectively, M. Kurz and J. Curtice for assistance in He isotope analysis, and F. Albarède and J. Blichert-Toft for introducing one of us (NM) to Hf isotopic analyses. J. Barling, C. Chauvel, A.D. Saunders, R. Rudnick, and W. M. White are thanked for their reviews that significantly improved the manuscript. Logistical support for the Kerimis cruise was provided by the Institut Français pour la Recherche et la Technologie Polaires (IFRTP) and the Institut Français de Recherche pour l'Exploitation de la Mer (IFREMER). We thank Commandant Gauthier and the crew of the M/V Marion Dufresne 2 and the GENAVIR and IFRTP teams for their outstanding contributions on board. EOST contribution 2002.11-UMR7516.

References

Albarède, F., Géochronologie comparée par la méthode ^{39}Ar-^{40}Ar de deux régions d'histoire post-hercynienne différente; La Montagne Noire et les Pyrénées orientales. Thesis, Univ. Paris 7, 1976.

Albarède, F., B. Luais, G. Fitton, M. Semet, E. Kaminski, B. G. J. Upton, P. Bachèlery, and J.-L. Cheminée, The geochemical regimes of Piton de la Fournaise volcano (Réunion) during the last 530,000 years, *J. Petrol.*, *38*, 171–201, 1997.

Barling, J., S. L. Goldstein, and I. A. Nicholls, Geochemistry of Heard Island (Southern Indian Ocean): Characterization of an enriched mantle component and implications for enrichment of the sub-Indian Ocean mantle, *J. Petrol.*, *35*, 1017–1053, 1994.

Barron, J., B. Larsen, and Shipboard Scientific Party, *Proceedings of Ocean Drilling Program, Inital Reports,* vol. 119, Ocean Drill. Program, College Station, Tex., 1989.

Blichert-Toft, J., C. Chauvel, and F. Albarède, Separation of Hf and Lu for high-precision isotope analysis of rock samples by magnetic sector-multiple collector ICP-MS, *Contrib. Mineral. Petrol.*, *127*, 248–260, 1997.

Borisova, A. Y., I. K. Nikogosian, J. S. Scoates, D. Weis, D. Damasceno, N. Shimizu, and J. L. Touret, Melt, fluid and crystal inclusions in olivine phenocrysts from Kerguelen plume-derived picritic basalts: Evidence for interaction with the Kerguelen Plateau lithosphere, *Chem. Geol.*, *183*, 195–220, 2002.

Clarke, I., I. McDougall, and D. J. Whitford, Volcanic evolution of Heard and McDonald Islands, Southern Indian Ocean, in *Antarctic Earth Science*, edited by R. L. Oliver,

P. R. James, and J. B. Jago, pp. 631–635, Aust. Acad. of Sci., Canberra, 1983.

Class, C., and S. L. Goldstein, Plume-lithosphere interactions in the ocean basins: Cconstraints from the source mineralogy, *Earth Planet. Sci. Lett.*, *150*, 245–260, 1997.

Coffin, M. F., and O. Eldhom, Large igneous provinces: Crustal structure, dimensions, and external consequences, *Rev. Geophys.*, *32*(1), 1–36, 1994.

Coffin, M. F., H. L. Davies, and W. F. Haxby, Structure of the Kerguelen Plateau province from Seasat altimetry and seismic reflection data, *Nature*, *324*, 134–136, 1986.

Coffin, M. F., et al., *Kerguelen Plateau-Broken Ridge, Sites 1135–1142*, Ocean Drill. Prog., College Station, Tex., 2000.

Condomines, M., K. Gronvold, P. J. Hooker, K. Muehlenbachs, R. K. O'Nions, N. Oskarsson, and E. R. Oxburgh, Helium, oxygen, strontium and neodymium isotopic relationships in Icelandic volcanics, *Earth Planet. Sci. Lett.*, *66*, 125–136, 1983.

Cox, A., and G. B. Dalrymple, Statistical analysis of geomagnetic reversal data and the precision of potassium-argon dating, *J. Geophys. Res.*, *72*, 2603–2614, 1967.

Davies, H. L., S.-S. Sun, F. A. Frey, I. Gautier, M. T. McCulloch, R. C. Price, Y. Bassias, C. T. Klootwijk, and L. Leclaire, Basalt basement from the Kerguelen Plateau and the trail of a Dupal plume, *Contrib. Mineral. Petrol.*, *103*, 457–469, 1989.

Dosso, L., H. Bougault, P. Beuzart, J. Y. Calvez, and J. L. Joron, The geochemical structure of the South-East Indian ridge, *Earth Planet. Sci. Lett.*, *88*, 47–59, 1988.

Duncan, R. A., and M. S. Pringle, Basement ages from the Northern Kerguelen Plateau and Broken Ridge, *Eos Trans. AGU*, *81*(17), Spring Meet., Suppl., S424, 2000.

Duncan, R. A., and M. A. Richards, Hot spots, mantle plumes, flood basalts, and true polar wander, *Rev. Geophys.*, *29*(1), 31–50, 1991.

Duncan, R. A., and M. Storey, The life cycle of Indian Ocean hot spots, in *The Indian Ocean: A synthesis of results from the Ocean Drilling Program*, *Geophys. Monogr. Ser.*, vol. 70, edited by R. A. Duncan et al., pp. 91–103, AGU, Washington, D.C., 1992.

Frey, F. A., W. B. Jones, H. Davies, and D. Weis, Geochemical and petrologic data for basalts from Sites 756, 757, and 758: Implications for the origin and evolution of Ninety east Ridge, *Proc. Ocean Drill. Program Sci. Results*, *121*, 611–659, 1991.

Frey, F. A., M. F. Coffin, P. J. Wallace, D. Weis, X. Zhao, S. W. Wise Jr., V. Wähnert, D. A. H. Teagle, P. J. Saccocia, D. N. Reusch, M. S. Pringle, K. E. Nicolaysen, C. R. Neal, R. D. Müller, C. L. Moore, J. J. Mahoney, L. Keszthelyi, H. Inokuchi, R. A. Duncan, H. Delius, J. E. Damuth, D. Damasceno, H. K. Coxall, M. K. Borre, F. Boehm, J. Barling, N. T. Arndt, and M. Antretter, Origin and evolution of a submarine large igneous province: The Kerguelen Plateau and Broken Ridge, southern Indian Ocean, *Earth Planet. Sci. Lett.*, *176*, 73–89, 2000a.

Frey, F. A., D. Weis, H.-J. Yang, K. Nicolaysen, H. Leyrit, and A. Giret, Temporal geochemical trends in Kerguelen Archipelago basalts: Evidence for decreasing magma supply from the Kerguelen Plume, *Chem. Geol.*, *164*, 61–80, 2000b.

Garcia, M. O., Petrography and olivine and glass chemistry of lavas from the Hawaiian Scientific Drilling Project, *J. Geophys. Res.*, *101*, 11701–11713, 1996.

Gautier, I., D. Weis, J.-P. Mennessier, P. Vidal, A. Giret, and M. Loubet, Petrology and geochemistry of Kerguelen basalts (South Indian Ocean): Evolution of the mantle sources from ridge to an intraplate position, *Earth Planet. Sci. Lett.*, *100*, 59–76, 1990.

Graham, D. W., K. T. M. Johnson, L. Douglas Priebe, and J. E. Lupton, Hot spot-ridge interaction along the Southeast Indian Ridge near the Amsterdam and St. Paul islands: Helium isotope evidence, *Earth Planet. Sci. Lett.*, *167*, 297–310, 1999.

Grégoire, M., J.-Y. Cottin, N. Mattielli, A. Giret, and D. Weis, Meta-igneous xenoliths from Kerguelen Archipelago: Deep magmatic intrusions equilibrated in granulite facies in an oceanic environment, *Contrib. Mineral. Petrol.*, *133*, 259–283, 1998.

Grove, T. L., D. C. Gerlach, and T. W. Sando, Origin of calc-alkaline series lavas at Medicine Lake Volcano by fractionation, assimilation and mixing, *Contrib. Mineral. Petrol.*, *80*, 160–182, 1982.

Hamelin, B., B. Dupré, and C. J. Allègre, Pb-Sr-Nd isotopic data of Indian Ocean Ridges: New evidence of large-scale mapping of mantle heterogeneities, *Earth Planet. Sci. Lett.*, *76*, 288–298, 1985/1986.

Henry, P., B. Azambre, R. Montigny, M. Rossy, and R. K. Stevenson, Late mantle evolution of the Pyrenean sub-continental lithospheric mantle in the light of new ^{40}Ar-^{39}Ar and Sm-Nd ages on pyroxenites and peridotites (Pyrenees, France), *Tectonophysics*, *296*, 103–123, 1998.

Hilton, D. R., J. Barling, and G. E. Wheller, Effect of shallow-level contamination on the helium isotope systematics of ocean-island lavas, *Nature*, *373*, 330–333, 1995.

Hofmann, A. W., and W. M. White, Mantle plumes from ancient oceanic crust, *Earth Planet. Sci. Lett.*, *57*, 421–436, 1982.

Houtz, R. E., D. E. Hates, and R. G. Markl, Kerguelen Plateau bathymetry, sediment distribution, and crustal structure, *Mar. Geol.*, *25*, 95–130, 1977.

Ila, P., and F. A. Frey, Trace element analysis of USGS standards AGV2, BCR2, BHVO2, DTS2 and GSP2 by INAA, *J. Radioanal. Nucl. Chem.*, *244*, 599–602, 2000.

Ingle, S. P., D. Weis, F. A. Frey, K. Nicolaysen, J. S. Scoates, and R. A. Duncan, Evidence for assimilation of continental crust by plume-derived basaltic magmas during formation of Elan Bank, Kerguelen Plateau: Results from Site 1137, ODP Leg 183, *Eos Trans. AGU*, *81*(17), Spring Meet. Suppl., S425, 2000.

Kieffer, B., N. T. Arndt, D. Weis, D. Bosch, D. Ayalew, G. Yirgu, and E. Ketefo, Petrology and geochemistry of the transition from tholeiitic flood basalts to alkaline shield volcanics in Ethiopia and Kerguelen, *Eos Trans. AGU*, *81*(17), Spring Meet. Suppl., S424, 2000.

Kurz, M. D., and W. J. Jenkins, The distribution of helium in oceanic basalt glasses, *Earth Planet. Sci. Lett.*, *53*, 41–54, 1981.

Kurz, M. D., W. J. Jenkins, J. G. Schilling, and S. R. Hart, Helium isotopic variations in the mantle beneath the central North Atlantic Ocean, *Earth Planet. Sci. Lett.*, *58*, 1–14, 1982.

Kurz, M. D., W. J. Jenkins, S. R. Hart, and D. Clague, Helium isotopic variations in volcanic rocks from Loihi seamount and the island of Hawaii, *Earth Planet. Sci. Lett.*, *66*, 388–406, 1983.

Kurz, M. D., T. Kenna, J. Lassiter, and D. J. DePaolo, Helium isotopic evolution of Mauna Kea volcano: First results from the 1 km drill core, *J. Geophys. Res.*, *101*(B5), 11,781–11,791, 1996.

Leclaire, L., Y. Bassias, M. Denis-Clocchiatti, H. Davies, I. Gautier, and J. Wannesson, Lower Cretaceous basalt and sediment from the Kerguelen Plateau, *Geo. Mar. Lett.*, *7*, 169–176, 1987.

MacDonald, G. A., and T. Katsura, Chemical composition of Hawaiian lavas, *J. Petrol.*, *5*, 82–133, 1964.

Mahoney, J., A. P. Le Roex, Z. Peng, R. L. Fisher, and J. H. Natland, Southwestern limits of Indian Ocean ridge mantle and the origin of low $^{206}Pb/^{204}Pb$ mid-ocean ridge basalt: Isotope systematics of the central southwest Indian ridge (17°-50°E), *J. Geophys. Res.*, *97*(B13), 19,771–19,790, 1992.

Mahoney, J. J., W. B. Jones, F. A. Frey, V. J. M. Salters, D. G. Pyle, and H. L. Davies, Geochemical characteristics of lavas from Broken Ridge, the Naturaliste Plateau and southernmost Kerguelen plateau: Cretaceous plateau volcanism in the southeast Indian Ocean, *Chem. Geol.*, *120*, 315–345, 1995.

Mahoney, J. J., R. Frei, M. L. G. Tejada, X. X. Mo, P. T. Leat, and T. F. Nägler, Tracing the Indian Ocean mantle domain through time: Isotopic results from old West Indian, East Tethyan, and South Pacific seafloor, *J. Petrol.*, *39*, 1285–1306, 1998.

Mattielli, N., D. Weis, S. Ingle, J. Blichert-Toft, and J. Barling, Hafnium isotopic constraints on the source of Kerguelen Plateau lavas (Leg 183 Sites 1140 and 1137), *Eos Trans. AGU*, *81*(17), Spring Meet. Suppl., S430, 2000.

Michard, A., R. Montigny, and R. Schlich, Geochemistry of the mantle below the Rodriquez Triple junction and the South-East Indian Ridge, *Earth Planet. Sci. Lett.*, *78*, 104–114, 1986.

Montigny, R., O. Le Mer, R. Thuizat, and H. Whitechurch, K-Ar and $^{40}Ar/^{39}Ar$ study of metamorphic rocks associated with the Oman ophiolite: Tectonic implications, *Tectonophysics*, *151*, 345–362, 1988.

Müller, R. D., J. Y. Royer, and L. A. Lawver, Revised plate motions relative to the hot spots from combined Altantic and Indian Ocean hot spot tracks, *Geology*, *21*, 275–278, 1993.

Munschy, M., and R. Schlich, Structure and evolution of the Kerguelen-Heard Plateau (Indian Ocean) deduced from seismic stratigraphy studies, *Mar. Geol.*, *76*, 131–152, 1987.

Munschy, M., B. Fritsch, R. Schlich, and Y. Rotstein, Tectonique extensive sur le plateau de Kerguelen, *Mem. Soc. Geol. Fr.*, *166*, 99–108, 1994.

Nicolaysen, K., F. A. Frey, M. Kurz, D. Weis, H. Leyrit, and A. Giret, $^{3}He/^{4}He$ ratios in Kerguelen Archipelago basalts: New evidence for an undegassed mantle plume component, *Mineral. Mag.*, *62A*, 1083–1084, 1998.

Nicolaysen, K., F. A. Frey, K. Hodges, D. Weis, and A. Giret, $^{40}Ar/^{39}Ar$ geochronology of flood basalts, from the Kerguelen Archipelago, southern Indian Ocean: Implications for Cenozoic eruptive rates of the Kerguelen Plume, *Earth Planet. Sci. Lett.*, *174*, 313–328, 2000.

Nicolaysen, K., S. Bowring, F. Frey, D. Weis, S. Ingle, M. S. Pringle, M. F. Coffin, and Leg 183 Shipboard Scientific Party, Provenance of Proterozoic garnet-biotite gneiss recovered from Elan Bank, Kerguelen Plateau, southern Indian Ocean, *Geology*, *29*, 235–238, 2001.

Poreda, R., J. G. Schilling, and H. Craig, Helium and hydrogen isotopes in ocean-ridge basalts north and south of Iceland, *Earth Planet. Sci. Lett.*, *78*, 1–17, 1986.

Price, R. C., A. K. Kennedy, M. Riggs-Sneeringer, and F. A. Frey, Geochemistry of basalts from the Indian Ocean triple junction: Implications for the generation and evolution of Indian Ocean ridge basalts, *Earth Planet. Sci. Lett.*, *78*, 379–396, 1986.

Pringle, M. C., and R. A. Duncan, Basement ages from the Southern and Central Kerguelen Plateau: Initial products of the Kerguelen Large Igneous Province, *Eos Trans. AGU*, *81*(17), Spring Meet. Suppl., S424, 2000.

Quilty, P. G., S. Shafik, A. McMinn, H. Brady, and I. Clarke, Microfossil evidence for the age and environment of deposition of sediments of Heard and McDonald Islands, in *Antarctic Earth Science*, edited by R. L. Oliver, P. R. James, and J. B. Jago, pp. 636–639, Aust. Acad. of Sci., Canberra, 1983.

Rhodes, J. M., Geochemical stratigraphy of lava flows samples by the Hawaii Scientific Drilling Project, *J. Geophys. Res.*, *101*(B5), 11,729–11,746, 1996.

Roeder, P. L., and R. F. Emslie, Olivine-liquid equilibrium, *Contrib. Mineral. Petrol.*, *29*, 275–289, 1970.

Salters, V. J. M., and W. M. White, Hf isotope constraints on mantle evolution, *Chem. Geol.*, *145*, 447–460, 1998.

Salters, V. J. M., M. Storey, J. H. Sevigny, and H. Whitechurch, Trace element and isotopic characteristics of Kerguelen-Heard plateau basalts, *Proc. Ocean Drill. Program Sci. Res.*, *120*, 55–62, 1992.

Schlich, R., The Indian Ocean: Aseismic ridges, spreading centers and oceanic basins, in *The Ocean Basins and Margins,* vol. 6, edited by A. E. M. Nairn and F. G. Stehli, pp. 51–148, Plenum, New York, 1982.

Schlich, R., J. R. Delteil, J. Moulin, P. Patriat, and R. Guillaume, Mise en évidence d'une sédimentation de marge continentale sur le plateau de Kerguelen-Heard, *C.R. Acad. Sci. Paris*, *272*, 2060–2063, 1971.

Schlich, R., S. W. J. Wise, and Shipboard Scientific Party, *Proceedings of Ocean Drilling Program, Inital Reports*, vol. 120, Ocean Drill. Program, College Station, Tex., 1989.

Schlich, R., M. Schaming, D. Weis, R. Montigny, and D. Damasceno, New structural and tectonic data in the Northern Kerguelen Plateau, *Eos Trans. AGU*, *79*(46), Fall Meet. Suppl., F871, 1998.

Seidemann, D. E., Effects of submarine alteration on K-Ar dating of deep-sea igneous rocks, *Geol. Soc. Am. Bull.*, *88*, 1660–1666, 1977.

Steiger, R. H., and E. Jäger, Subcommission on Geochronology: Convention of the use of decay constants in geo- and cosmochronology, *Earth Planet. Sci. Lett.*, *36*, 359–362, 1977.

Steinberger, B., Plumes in a convecting mantle: Models and observations for individual hot spots, *J. Geophys. Res.*, *105*(B5), 11,127–11,152, 2000.

Storey, M., R. Kent, A. D. Saunders, V. J. Salters, J. Hergt, H. Whitechurch, J. H. Sevigny, M. F. Thirwall, P. Leat, N. C. Ghose, and M. Gifford, Lower Cretaceous volcanic rocks along continental margins and their relationship to the Kerguelen Plateau, *Proc. Ocean Drill. Program Sci. Res.*, *120*, 33–53, 1992.

Sun, S.-S., and W. F. McDonough, Chemical and isotopic systematics of oceanic basalts: Implications for mantle composition and processes, in *Magmatism in the Ocean Basins*, vol. 42, edited by A. D. Saunders and M. J. Norry, pp. 313–345, Blackwell Sci., Malden, Mass., 1989.

Turner, G., S. F. Knott, R. D. Ash, and J. D. Gilmour, Ar-Ar chronology of the Martian meteorite ALH84001: Evidence for the timing of the early bombardment of Mars, *Geochim. Cosmochim. Acta*, *61*, 3835–3850, 1997.

Vance, D., J. O. H. Stone, and R. K. O'Nions, He, Sr and Nd isotopes in xenoliths from Hawaii and other oceanic islands, *Earth Planet. Sci. Lett.*, *96*, 147–160, 1989.

Weis, D., and F. A. Frey, Isotope geochemistry of Ninety east Ridge basalts: Sr, Nd, and Pb evidence for the involvement of the Kerguelen hot spot, *Proc. Ocean Drill. Program Sci. Res.*, *121*, 591–610, 1991.

Weis, D., and F. A. Frey, Role of the Kerguelen Plume in generating the eastern Indian Ocean seafloor, *J. Geophys. Res.*, *101*(B6), 13,381–13,849, 1996.

Weis, D., and F. A. Frey, ODP Site 1140 on the Northern Kerguelen Plateau: 34 Ma Pillow Basalts Related to the Kerguelen Plume and the Southeast Indian Ridge, *Eos Trans. AGU*, *81*(17), Spring Meet. Suppl., S425, 2000.

Weis, D., and A. Giret, Kerguelen plutonic complexes: Sr, Nd, Pb isotopic study and inferences about their sources, ages and geodynamic setting, *Bull. Soc. Geol. Fr.*, *166*, 47–59, 1994.

Weis, D., D. Demaiffe, S. Cauët, and M. Javoy, Sr, Nd, O and H isotopic ratios in Ascension Island lavas and plutonic inclusions: Cogenetic origin, *Earth Planet. Sci. Lett.*, *82*, 255–268, 1987.

Weis, D., Y. Bassias, I. Gautier, and J.-P. Mennessier, Dupal anomaly in existence 115 Ma ago: Evidence from isotopic study of the Kerguelen Plateau (South Indian Ocean), *Geochim. Cosmochim. Acta*, *53*, 2125–2131, 1989a.

Weis, D., J.-F. Beaux, I. Gautier, A. Giret, and P. Vidal, Kerguelen Archipelago: Geochemical evidence for recycled material, in *Crust/Mantle Recycling at Convergence Zones*, edited by S. R. Hart and L. Gülen, pp. 59–63, Kluwer Acad. Norwell, Mass., 1989b.

Weis, D., F. A. Frey, A. Saunders, I. Gibson, and Leg 121 Shipboard Scientific Party, Ninety east Ridge (Indian Ocean): A 5000 km record of a Dupal mantle plume, *Geology*, *19*, 99–102, 1991.

Weis, D., F. A. Frey, H. Leyrit, and I. Gautier, Kerguelen Archipelago revisited: Geochemical and isotopic study of the SE Province lavas, *Earth Planet. Sci. Lett.*, *118*, 101–119, 1993.

Weis, D., D. Damasceno, F. A. Frey, K. Nicolaysen, and A. Giret, Temporal isotopic variations in the Kerguelen Plume: Evidence from the Kerguelen Archipelago, *Mineral. Mag.*, *62A*, 1643–1644, 1998a.

Weis, D., F. A. Frey, A. Giret, and J. M. Cantagrel, Geochemical characteristics of the youngest volcano (Mount Ross) in the Kerguelen Archipelago: Inferences for magma flux and composition of the Kerguelen Plume, *J. Petrol.*, *39*, 973–994, 1998b.

Weis, D., S. Ingle, K. Nicolaysen, F. A. Frey, D. Damasceno, J. Barling, and Leg 183 Shipboard Scientific Party, Origin of continental components in Indian Ocean basalts: Evidence from Elan Bank (Kerguelen Plateau, ODP Leg 183, Site 1137), *Geology*, *29*, 147–150, 2001.

Yang, Y. J., F. A. Frey, K. Nicolaysen, D. Weis, and A. Giret, Petrogenesis of flood basalts forming the Northern Kerguelen Archipelago: Implications for the Kerguelen Plume, *J. Petrol.*, *39*, 711–748, 1998.

Zindler, A., and S. R. Hart, Chemical geodynamics, *Ann. Rev. Earth Plan. Sci.*, *14*, 493–571, 1986.